Highlights

Redundancy parameterization and inverse kinematics of 7-DOF revolute manipulators

Alexander J. Elias, John T. Wen

- A new robot redundancy parameterization has a singularity only along a half-line
- New stereographic shoulder-elbow-wrist angle Jacobian and singularities found
- Algorithmic singularities are unavoidable for any redundancy parameterization
- Inverse kinematics efficiently solved for 7-degree-of-freedom revolute manipulators
- Search-based inverse kinematics solutions may be converted to polynomial root finding

Redundancy parameterization and inverse kinematics of 7-DOF revolute manipulators

Alexander J. Elias[*], John T. Wen

Department of Electrical, Computer, and Systems Engineering, Rensselaer Polytechnic Institute, 110 8th St, Troy, NY 12180, United States

Abstract

Seven-degree-of-freedom (DOF) robot arms have one redundant DOF for obstacle and singularity avoidance which must be parameterized to fully specify the joint angles for a given end effector pose. Commonly used 7-DOF revolute (7R) industrial manipulators from ABB, Motoman, and KUKA and space manipulators like SSRMS or FREND are conventionally parameterized by the shoulder-elbow-wrist (SEW) angle for path planning and teleoperation. We introduce the general SEW angle which generalizes the conventional SEW angle with an arbitrary reference direction function. Redundancy parameterizations such as the conventional SEW angle encounter an algorithmic singularity along a line in the workspace. We introduce a reference direction function choice called the stereographic SEW angle which has a singularity only along a half-line which can be out of reach, enlarging the usable workspace. We prove all parameterizations have an algorithmic singularity. Finally, using the general SEW angle and subproblem decomposition, we provide efficient singularity-robust inverse kinematics solutions which are often closed-form but may involve a 1D or 2D search. Search-based solutions may be converted to finding polynomial roots. Examples are available in a publicly accessible repository.

Keywords: Kinematics, Redundant robots, Industrial robots, Space robotics and automation, Telerobotics and teleoperation, Humanoid robot systems

1. Introduction

Most industrial robot arms have six revolute joints to control the six degrees of freedom (DOF) of the robot end effector pose, but a human arm has seven DOF: three for the shoulder, one for the elbow, and three for the wrist. Similarly, there are 7-DOF revolute (7R) robot arms such as the Robotics Research Corporation (RRC) arm [1], Baxter [2], Sawyer [3], YuMi [4], and the Space Station Robot Manipulator System (SSRMS) [5]. The extra *redundant* degree of freedom means there is a continuum of arm configurations for a given hand or robot end effector pose. Holding the end effector pose constant while moving through the continuum of arm configurations, called self-motion, commonly looks like the elbow rotating around the line passing from the shoulder to the wrist (Fig. 1). Benefits of 7R arms over 6R arms include using redundancy to avoid singularities and obstacles [6], optimize motion time [7], avoid joint motion limits [8], and avoid joint torque limits [9].

To fully specify the pose of a 7R robot up to a finite number of solutions, the end effector pose must be augmented by a secondary task. During pure self-motion, the only difference between parameterizations would be the rate of movement; differences between parameterizations are made clearer during motion of the end effector. Redundancy in human and many 7R robot arms may be conveniently parameterized by the shoulder-elbow-wrist (SEW) angle, sometimes called the elbow angle, which characterizes the rotation of the plane containing the shoulder, elbow, and wrist about the shoulder-wrist line with respect to a reference plane. This reference plane is conventionally chosen to contain the shoulder-wrist line and a reference vector. This redundancy parameterization is easy to visualize and is

[*]Corresponding author

Email addresses: `eliasa3@rpi.edu` (Alexander J. Elias), `wenj@rpi.edu` (John T. Wen)

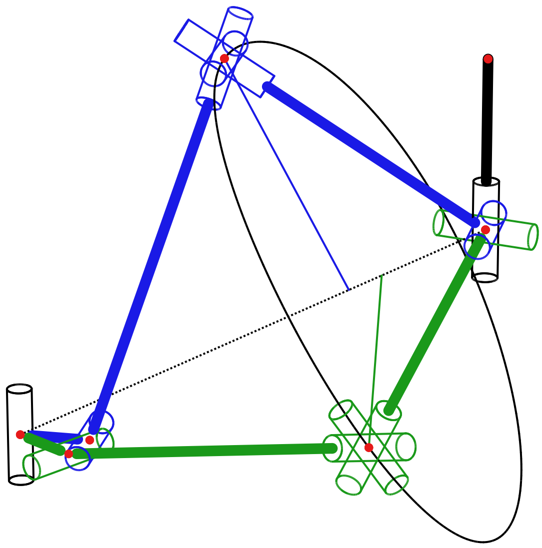

Fig. 1. Self-motion for a Motoman SIA50D [14] (R-R-3R$^{\text{E}}$-2R) robot arm. For a given end effector pose, the spherical elbow may be on a curve which is the intersection of a torus formed by joints 1 and 2 and a sphere centered at joints 6 and 7.

widely used industrially and in applications such as space teleoperation [10, 11, 12] partly because it is intuitive for space robot operators [13]. Furthermore, for certain 7R arms, the inverse kinematics (IK) has an analytical solution, i.e., for a given robot end effector pose and SEW angle, the finite set of the seven robot joint angles may be solved directly instead of iteratively. The augmented Jacobian, the 7×7 matrix that maps the joint velocity vector to the end effector spatial velocity and the SEW angular velocity, is easily characterized.

An issue with the conventional SEW angle becomes apparent when the shoulder-wrist line is collinear with the reference vector because the reference plane becomes undefined. This is referred to as an *algorithmic singularity*, a singularity due to the choice of redundancy parameterization.

Algorithmic singularities are the main weakness of parameterizations like the SEW angle [15] because robots experience undesirable behavior near them just as for kinematic singularities. For example, being near an algorithmic singularity may result in dangerously large elbow movement which is especially problematic for teleoperation [10]. It also leads to poor convergence for iterative algorithms as well as numerical precision problems since many significant digits are required to accurately specify the robot pose. Designers must carefully choose the reference direction to avoid singularities, but it is often inevitable to waste regions of the reachable workspace [16, 17, 18, 19].

In this paper, we introduce a new generalized SEW angle which includes the conventional SEW angle as a special case. We show that an algorithmic singularity is unavoidable for any redundancy parameterization, but a special choice of the generalized SEW angle based on the stereographic projection changes the bidirectional singularity to a unidirectional singularity. The singularity direction may be located towards the base of the arm so it will not be encountered in the robot workspace. The advantages of the conventional SEW angle redundancy parameterization are still retained for the generalized SEW angle, including analytical inverse kinematics for many 7R arms, intuitive teleoperation, and an analytical Jacobian. Most existing algorithms that use the conventional SEW angle or its Jacobian can be easily adapted to use the general SEW angle, including the stereographic SEW angle.

We also provide inverse kinematics solutions using the general SEW angle for most 7R robots used in practice or mentioned in the literature including general 7R manipulators, as well as arms that do not yet exist. These solutions are built upon IK-Geo, an open-source and easy-to-use IK solver based on a unifying subproblem decomposition approach [20]. The solutions are often closed-form, but for some robots, IK is solved using a 1D or 2D search over a compact set.

These analytical and semi-analytical methods are efficient, precise, and stable, especially compared to Jacobian-based algorithms. They are also robust to singularities and find all IK solutions, including singular solutions, rather than just one close to an initial guess. For branches without exact solutions, they return continuous non-exact and sometimes least-squares solutions. This allows Cartesian motion directly through singularities to switch between different IK branches without resorting to joint control. We also demonstrate converting a search-based solution to a polynomial solution: To the best of our knowledge, we are the first to provide a polynomial in the tangent half-angle of one joint which corresponds to IK solutions of a 7R robot parameterized by SEW angle.

We offer the following new contributions in this paper:

- We introduce the stereographic SEW angle, a new redundancy parameterization that encounters a singularity only along a half-line instead of a full line as in the conventional SEW angle. This significantly enlarges the singularity-free region of the workspace.
- We show algorithmic singularities are unavoidable for any redundancy parameterization. We classify different types of singularities for 7R arms and discuss when singularities are concurrent.
- We efficiently solve IK for any 7R manipulator parameterized by the conventional or stereographic SEW angle using the subproblem decomposition approach. We categorize 7R robots based on intersecting or parallel axes and choices of shoulder, elbow, and wrist locations. We also demonstrate solving IK for a 7R manipulator parameterized by conventional or stereographic SEW angle by finding a high-order polynomial in the tangent half-angle of one joint.

The remainder of the paper is organized as follows. In Section 2 we discuss previous related works, and we describe forward kinematics for 7R arms using coordinate-free notation and the product of exponentials approach. We introduce the general SEW angle in Section 3 including forward and differential kinematics, we discuss singularity conditions, and we relate it to the conventional SEW angle. In Section 4 we prove the existence of algorithmic singularities for any redundancy parameterization. We define the stereographic SEW angle in Section 5, discuss its relationship to stereographic projection and its singularity behavior, and provide an example comparing the conventional and stereographic SEW angle formulations. We provide IK solutions with examples in Section 6, and we conclude in Section 7.

Inverse kinematics solutions, examples, and evaluations are available in a publicly accessible repository[1].

2. Background

2.1. Robot notation

To notate different families of robot kinematic parameters, we follow and slightly extend the notation introduced by [21]. A single revolute joint is notated by R, and when multiple joints intersect, they may be notated as 2R or 3R for two or three intersecting joints, respectively. The joints are written in order from the base to the end effector. For example, a robot with a spherical shoulder, a revolute elbow, and a spherical wrist may be notated as 3R-R-3R. We also introduce the notation of 2R|| and 3R|| to indicate two or three consecutive parallel revolute joints. Note that since a given joint may intersect or be parallel with both the joint before it and the joint after it, a single robot may fall into multiple robot kinematic families.

We use superscript S, E, or W to indicate when the shoulder, elbow, or wrist is placed at a joint or joint intersection. For example, $2R^E$ would indicate a 2R joint with the elbow placed at the joint intersection. Unless otherwise indicated, a robot has its shoulder on the first joint or joint intersection and has its wrist on its last joint or joint intersection.

2.2. Related literature

The analysis and parameterization of the redundant degree of freedom in 7R manipulators has been primarily driven by space robotics applications and more recently motivated by industrial robots in manufacturing and humanoid robots. Early papers focused on analyzing the geometry, topology, and differential kinematics of 7-DOF manipulators. [22] introduced the concept of the augmented Jacobian (termed the extended Jacobian) and discussed the algorithmic singularity. [6] discussed options for 7-DOF manipulator designs, including how adding an extra degree of freedom

[1] `https://github.com/rpiRobotics/stereo-sew`

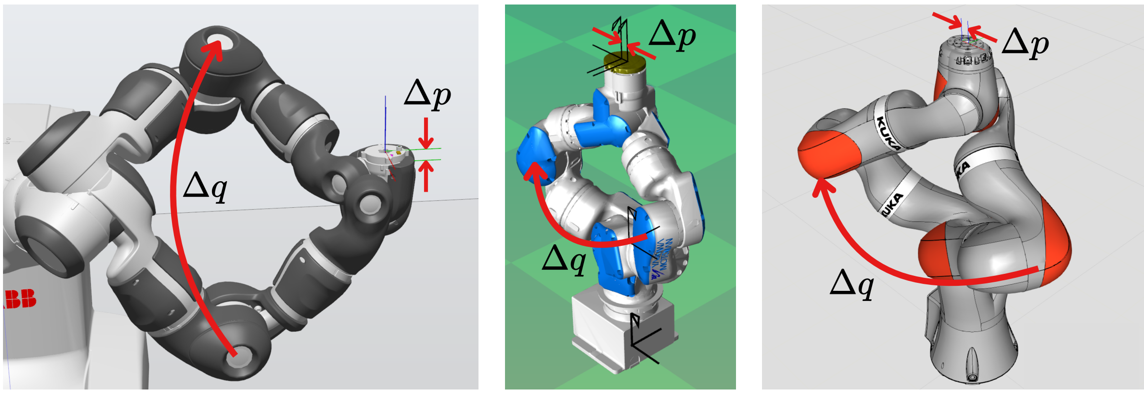

(a) ABB. **(b)** Yaskawa Motoman. **(c)** KUKA.

Fig. 2. The conventional SEW angle is used in industrial manipulators to parameterize the redundant degree of freedom. The algorithmic singularity results in large elbow movement Δq for small changes in the end effector pose Δp while keeping the SEW angle constant.

removes internal singularities. The paper discusses the self-motion manifold and was one of the earliest papers to recommend using the conventional SEW angle (with the reference vector pointing up). [23] gave an overview of the topology of the self-motion manifold. [24, 25] provided a detailed analysis of the conventional SEW angle with application to 3R-R-3R arms and the RRC arm, which has no intersecting consecutive joint axes. They also provided the expression for the SEW Jacobian and singularity analysis.

Parameterizing the redundant degree of freedom is not strictly necessary to control a 7R arm. For example, one can use resolved velocity or resolved acceleration control using the weighted or unweighted Jacobian pseudoinverse, or perform optimization of some other task that is not a function of joint angles. A critical problem with these controllers is non-cyclicity [13, 26]. These controllers are non-conservative, so if the robot makes a closed loop in its end effector path, the elbow may not return to its original position. This is unacceptable in industrial or mission-critical scenarios. Furthermore, these differential redundancy resolution techniques have stability problems: Minimizing joint velocity, joint torque, or joint acceleration locally does not prevent the robot from approaching a singularity [27, 9]. Extra work must be done to stabilize such a controller to prevent it from driving itself into a singularity [28].

On the other hand, augmenting the task space with a function of the joint angles, such as the SEW angle, ensures cyclical behavior and gives direct control of the redundant degree of freedom over the entire trajectory [29]. By using a global rather than local approach, task-space behavior is immediately known without using IK. This leads to intuitive teleoperation and programming and allows for transferring task-space behavior between robots or even between humans and robots [26, 30].

It is no wonder that the SEW angle is widely used for teleoperation in space [10, 12, 11], underwater [16, 17, 18, 19], and in surgery [31, 32, 33]. The conventional SEW angle is also widely used in industrial manipulators from companies like ABB, Yaskawa Motoman, and KUKA (Fig. 2). The ABB YuMi [4] is parameterized by the conventional SEW angle with a choice of three different reference vectors. Any of these choices result in a singularity in a line through the workspace. The robot controller does not allow for Cartesian motion, such as the `MoveL` command, near this singularity, which is made clear in the robot manual [34, Sec. 6.33.28]. Motoman robots such as the SIA5D [35] and KUKA robots such as the LBR iiwa 14 R820 [36] are parameterized by the conventional SEW angle with the reference vector pointing in the z direction. Large joint motion when the wrist passes by the reference vector means that Cartesian velocity is severely limited. Using the stereographic SEW angle rather than the conventional SEW angle would remove the algorithmic singularity from the reachable workspace while still maintaining cyclicity and ease of use for the robot operator.

The SEW angle allows for ease of global planning [11] since the entire solution space can be considered, and it can be easily extended to incorporate hybrid force-motion or impedance control of both end effector motion and self-motion [33, 31, 32, 37]. Additionally, the SEW angle is compatible with other optimizations to avoid obstacles, joint angle limits, joint torque limits, or singularities, or to maximize metrics like force transmission ratio [16, 17, 18, 19, 38, 39, 33, 31, 32]. There are also applications of the SEW angle not just to typical 7-DOF robots, but also to human arms and wearable robots [40, 41, 42, 43, 44, 45, 46, 47].

There have been several other proposed redundancy parameterizations besides the conventional SEW angle. [48] attempted to address the singularity issue of the conventional SEW angle by proposing a method that picks two different reference vectors and switches between the corresponding SEW angles when one of them encounters a singularity. The resulting parameterization is non-smooth, and singularities would still be present. Furthermore, this parameterization is no longer a function of the joint angles and will therefore be noncyclical. Similar issues occur for any other method that switches between parameterizations, such as the method proposed by [49] to switch between the SEW angle and the first joint angle. [50] used the SEW angle where the reference plane is formed by the elbow when joint three is zero. They explained the reference plane is undefined in a shoulder or elbow singularity, so there is no benefit in terms of singularity existence as compared to the conventional SEW angle. One can also parameterize the redundant DOF by choosing one joint angle and reducing the problem to the IK of a non-redundant 6R manipulator, but this introduces singularities resulting from the equivalent 6R robot. In fact, it appears that all proposed redundancy parameterizations up to now have a bidirectional singularity. This makes the stereographic SEW angle the only parameterization proposed so far with a unidirectional singularity structure.

Numerous authors have found the IK solutions of 7R arms parameterized by one joint angle. By parameterizing joint 1, authors have found the solutions to robots in the following kinematic families: R-R-3R-2R [51], 2R-2R-3R [49], 3R-R-3R [52], R-R-3R-2R [53], and R-2R-2R-2R (using 1D search) [54]. [55] found the IK solutions for a 3R-R-3R arm by parameterizing joint 2 or 3, and [56] found the IK solutions for a 2R-3R||-2R arm parameterized by any joint angle. In [57], the authors provide guidelines for which joints to parameterize in redundant robots based on several heuristics including maintaining spherical wrists, preventing degenerate manipulators, and avoiding the workspace shrinking after parameterization. It is worth noting that the IK problem for redundant robots parameterized by joint angles is equivalent to the 6-DOF robot IK problem which has its own extensive literature.

Many papers provide inverse kinematics solutions using the conventional SEW angle. [58, 59, 60] used the conventional SEW angle to provide closed-form IK for 3R-R-3R arms. [49] found a closed-form IK solution for 2R-2R-3R arms. Many papers used an iterative IK method with an approximate closed-form solution as a starting point: [61] for an R-2R-R-3R arm, and [62] for a 2R-3R||-2R arm. [63] also found an iterative solution for a 2R-3R||-2R. The paper states closed-form IK is not possible when using SEW angle. However, [64] solved IK for a 2R-3R||-2R manipulator in closed form by defining the SEW plane to be perpendicular to joint axes 3, 4, and 5.

Until now, no one has proposed a unified method of inverse kinematics for any 7R manipulator parameterized by the SEW angle that does not rely on the Jacobian.

2.3. Robot kinematics

We use the coordinate-free notation shown in Table 1. Vector $\vec{p}$ represented in frame $\mathcal{E}_a$ is the $\mathbb{R}^3$ vector $p_a = \mathcal{E}_a^* \vec{p}$, where

$$\mathcal{E}_a^* = \begin{bmatrix} \vec{e}_x \cdot \\ \vec{e}_y \cdot \\ \vec{e}_z \cdot \end{bmatrix} \tag{1}$$

is the adjoint of $\mathcal{E}_a$. Frame $\mathcal{E}_b$ represented in frame $\mathcal{E}_a$ is the $SO(3)$ matrix $R_{ab} = \mathcal{E}_a^* \mathcal{E}_b$. Rotation $\mathcal{R}(\vec{h}, \theta)$ in frame $\mathcal{E}_a$ is the $SO(3)$ matrix $\mathrm{R}(h_a, \theta) = e^{h_a^\times \theta}$, where $(\cdot)^\times$ is the 3×3 skew-symmetric matrix representation of the cross product:

$$h^\times := \begin{bmatrix} 0 & -h_z & h_y \\ h_z & 0 & -h_x \\ -h_y & h_x & 0 \end{bmatrix}. \tag{2}$$

For a unit vector h, $-h^{\times 2} = -h^\times h^\times = I - hh^T$ is the projector onto the orthogonal complement of h.

Consider a 7R robot as shown in Fig. 3 with joint angles $q = [q_1 \; q_2 \; \cdots \; q_7]^T$. We will use the product of exponentials approach to describe the arm kinematics. Denote the base frame and base frame origin as $(\mathcal{E}_0, \mathcal{O}_0)$ and the end effector task frame and task frame origin as $(\mathcal{E}_T, \mathcal{O}_T)$. Choose the link frame origins $\mathcal{O}_i$ along each unit joint

Table 1
Nomenclature.

Coordinate-Free Notation	
O	Point in Euclidean space.
$\vec{p}$	Vector in Euclidean space.
$\mathcal{E}$	Orthonormal frame, $= [\vec{e}_x\ \vec{e}_y\ \vec{e}_z]$.
$\mathcal{R}(\vec{h}, \theta)$	Rotation operator about $\vec{h}$ over angle θ.
Robot Kinematics	
O_S	Shoulder.
O_E	Elbow.
O_W	Wrist.
O_C	Center of rotation. Projection of elbow on shoulder-wrist line.
J	End effector Jacobian.
J_E	Elbow Jacobian.
J_W	Wrist Jacobian.
General SEW Angle	
k_{SEW}	$= p_{SW}^{\times} p_{SE}$.
n_{SEW}	$= k_{SEW} / \lVert k_{SEW} \rVert$. SEW plane normal.
ψ	SEW angle.
$e_x = f_x(p_{SW})$	Reference direction function.
(e_x, e_y, e_{SW})	SEW angle coordinate frame.
J_{f_x}	Reference direction Jacobian w.r.t. p_{SW}.
J_ψ	SEW angle Jacobian.
J_A	Augmented Jacobian.
Conventional SEW Angle	
e_r	Arbitrary unit reference vector.
k_y	$= p_{SW}^{\times} e_r$, meaning $e_y = k_y / \lVert k_y \rVert$.
Stereographic SEW Angle	
e_t	Unit translation vector.
k_{rt}	$= (e_{SW} - e_t)^{\times} e_r$.
k_x	$= k_{rt}^{\times} p_{SW}$, meaning $e_x = k_x / \lVert k_x \rVert$.

axis $\vec{h}_i$. Let $\vec{p}_{ij}$ be the vector from O_i to O_j. Define the ith frame $\mathcal{E}_i = \mathcal{R}(\vec{h}_i, q_i)\mathcal{E}_{i-1}$. Then the forward kinematics of the task frame represented in the base frame is

$$R_{0T} = R_{01}R_{12}R_{23}R_{34}R_{45}R_{56}R_{67}R_{7T}, \tag{3a}$$

$$p_{0T} = p_{01} + R_{01}p_{12} + R_{02}p_{23} + R_{03}p_{34} + R_{04}p_{45} + R_{05}p_{56} + R_{06}p_{67} + R_{07}p_{7T}, \tag{3b}$$

where $R_{ij} = R_{i,i+1} \cdots R_{j-1,j}$, h_i and $p_{i-1,i}$ are constant $\mathbb{R}^3$ vectors representing $\vec{h}_i$ and $\vec{p}_{i-1,i}$ in $\mathcal{E}_{i-1}$, $R_{i-1,i} = e^{h_i^{\times} q_i}$ is $\mathcal{R}(\vec{h}_i, q_i)$ represented in $\mathcal{E}_{i-1}$, R_{7T} is a constant $SO(3)$ matrix for the fixed wrist-tool transform, and p_{7T} is the constant tool offset in the 7 frame. The constant vectors h_i, $p_{i-1,i}$, p_{7T} and constant transform R_{7T} are obtained by putting the arm in the zero configuration $q = 0$.

Define three points O_S, O_E, and O_W to represent the robot shoulder, elbow, and wrist, respectively. The locations for these points are arbitrary, but different choices will lead to different inverse kinematics methods and different singularity structures. For easier inverse kinematics, O_S should be constant in the base frame and O_W should be constant in the 7 frame (which also means it is constant in the tool frame). O_E must be placed somewhere in the

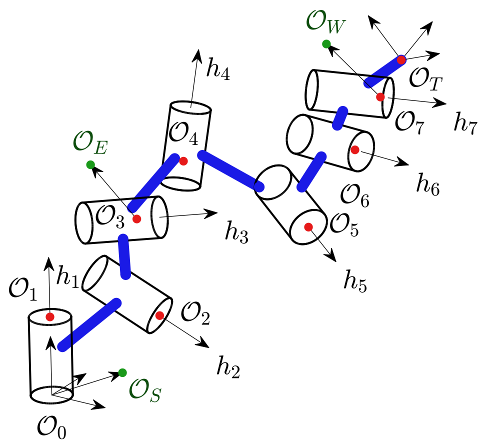

Fig. 3. General 7R robot arm with example shoulder, elbow, and wrist points O_S, O_E, and O_W fixed in $\mathcal{E}_0$, $\mathcal{E}_3$, and $\mathcal{E}_7$, respectively. In general, these points may be placed anywhere in the kinematic chain.

kinematic chain such that it rotates about the line passing through O_S and O_W as the robot moves through its redundant degree of freedom while keeping the end effector pose constant. For many robots, a good choice is to make O_E constant in frame $\mathcal{E}_3$ or $\mathcal{E}_4$. In this paper, we will use $\mathcal{E}_3$ for illustration. Representing these points in their respective constant frames, we have constant vectors p_{0S}, p_{3E}, and p_{7W}. For a given pose, we can find p_{SW} and p_{SE}, which are $\vec{p}_{SW}$ and $\vec{p}_{SE}$ represented in $\mathcal{E}_0$. The shoulder-wrist vector is

$$p_{SW} = p_{0T} - R_{07}p_{7T} + R_{07}p_{7W} - p_{0S}, \tag{4}$$

and the shoulder-elbow vector is

$$p_{SE} = p_{01} + R_{01}p_{12} + R_{02}p_{23} + R_{03}p_{3E} - p_{0S}. \tag{5}$$

It is often helpful for the inverse kinematics solution to set the shoulder, elbow, or wrist offset vector to 0 so that O_S, O_E, or O_W is coincident with the link frame origin.

On some robots, such as those with three consecutive parallel axes, it may be helpful to define the shoulder-elbow vector p_{SE} to be a unit vector e_{SE} which is equal to one of the joint axes represented in the base frame. For example, we may pick $p_{SE} = e_{SE} = R_{02}h_3$. Since three parallel joint axes are the limit of three intersecting axes where the point of intersection moves infinitely far away, this can be interpreted as choosing p_{SE} to be the normalized vector pointing at this intersection (Fig. 4). For some robots this leads to closed-form inverse kinematics using the subproblem decomposition approach.

3. General SEW Angle

3.1. Kinematics description

Consider a 7-DOF arm with shoulder, elbow, and wrist defined. The SEW (shoulder-elbow-wrist) angle ψ, also commonly referred to as the arm angle or swivel angle, is the angle of the shoulder-elbow vector p_{SE} about the shoulder-wrist vector p_{SW} with respect to some reference vector. Consider an arbitrary mapping, called the reference direction function, from the shoulder-wrist vector p_{SW} to a unit vector e_x which is orthogonal to p_{SW}. Denote this mapping by $e_x = f_x(p_{SW})$. From this we can form an orthonormal basis $(e_x,\ e_y,\ e_{SW})$, where e_{SW} is the normalized p_{SW} and $e_y = e_{SW}^{\times}e_x$. This frame may be used to measure the SEW angle.

There are two equivalent definitions of the SEW angle, as shown in Fig. 5. The elbow definition is that ψ is the angle between shoulder-elbow vector p_{SE} and reference vector e_x measured along the shoulder-wrist rotational axis e_{SW}. The plane definition is that ψ is the angle between n_{SEW}, which is the normal vector of the SEW plane containing the shoulder, elbow, and wrist, and e_y, which is the normal vector of the reference plane containing the

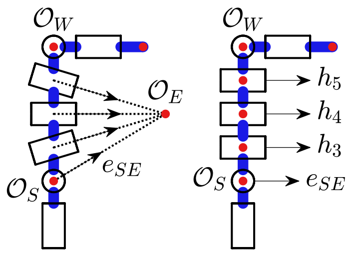

(a) 3R elbow. **(b)** 3R|| elbow.

Fig. 4. A 3R|| joint is the limit of a 3R joint as the intersection point moves to infinity. If this joint is the elbow, then although in the limit p_{SE} has infinite length, the normalized vector e_{SE} is defined and is equal to the three parallel joint axes.

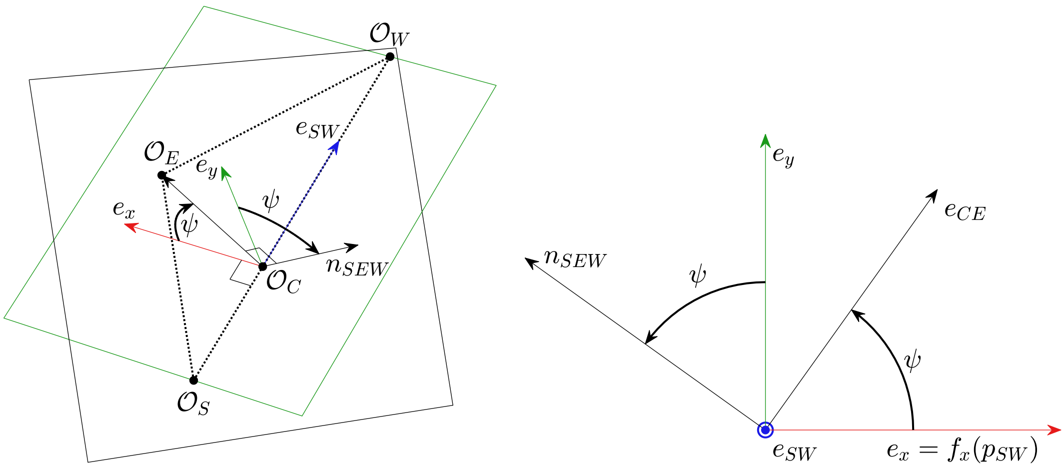

Fig. 5. The SEW angle ψ is the angle of the elbow measured from $e_x = f_x(p_{SW})$ about e_{SW}, which is also the angle of the SEW plane normal vector n_{SEW} measured from e_y about e_{SW}. In the general SEW angle, the reference direction function $f_x(p_{SW})$ is arbitrary but with the constraints that the output is unit length and orthogonal to p_{SW}.

shoulder, wrist, and reference vector e_x. While the elbow definition is helpful for forward kinematics, the plane definition is more useful for inverse kinematics when using the subproblem decomposition approach.

Using the elbow definition, the SEW angle is

$$\psi = \arg\min_{\theta} \|\mathrm{R}(e_{SW}, \theta)e_x - p_{SE}\| \,. \tag{6}$$

We can also rewrite this more compactly by removing the component of p_{SE} along e_{SW}. Let O_C, the center of rotation, be the point on p_{SW} such that p_{CE} is orthogonal to e_{SW}, i.e., the center-elbow vector is

$$p_{CE} = -e_{SW}^{\times 2} p_{SE}. \tag{7}$$

Then,

$$e_{CE} = \mathrm{R}(e_{SW}, \psi)e_x, \tag{8}$$

where the center-elbow direction vector is $e_{CE} = p_{CE}/\,\|p_{CE}\|$.

Using the plane definition, the SEW angle is

$$n_{SEW} = \mathrm{R}(e_{SW}, \psi)e_y, \tag{9}$$

where the normal of the plane containing the shoulder, elbow, and wrist is

$$n_{SEW} = \frac{k_{SEW}}{\|k_{SEW}\|}, \tag{10a}$$

$$k_{SEW} = p_{SW}^{\times} p_{SE}. \tag{10b}$$

Subproblem 1 [20] may be used to solve the forward kinematics for the SEW angle, which is

$$\psi = \text{atan2}\left(e_y^T p_{SE}, e_x^T p_{SE}\right) \tag{11a}$$

$$= \text{atan2}\left(e_y^T p_{CE}, e_x^T p_{CE}\right) \tag{11b}$$

$$= \text{atan2}\left(-e_x^T n_{SEW}, e_y^T n_{SEW}\right) \tag{11c}$$

$$= \text{atan2}\left(-e_x^T k_{SEW}, e_y^T k_{SEW}\right). \tag{11d}$$

To perform inverse kinematics, we can use a given end effector pose (R_{0T}, p_{0T}) to find p_{SW} from (4). Next, use the reference direction function $f_x(p_{SW})$ to find e_x or e_y. Then, for a given ψ, we can calculate e_{CE} or n_{SEW} using (8) or (9), respectively, which may then be used to determine the joint angle vector q. For the subproblem decomposition approach in Section 6, we always calculate n_{SEW}.

Some robots are not easily parameterized using the SEW angle. For example, the FANUC R-1000iA/120F-7B is an R-3R||-3R robot [65]. The redundant degree of freedom in this family of robots is the movement of joints 2, 3, and 4, along with the corresponding movement in the spherical wrist, which results in the shortening or lengthening of the distance between joints 2 and 4 [66]. However, with O_S placed at joint 1 and O_W placed at the spherical wrist, there is no movement of joints 2, 3, or 4 around e_{SW} during self-motion; they stay in the same half-plane and the SEW angle would fail to parameterize the redundant degree of freedom. Robots such as this are better parameterized by specifying a joint angle. (A good choice for this robot is q_3.)

To find the Jacobian of the SEW angle with respect to the joint angles, J_ψ, we will write it in terms of the partial Jacobians mapping joint angular velocities to the linear velocity of the elbow O_E and the wrist O_W:

$$\dot{p}_{SE} = \dot{p}_{0E} = J_E \dot{q}, \quad \dot{p}_{SW} = \dot{p}_{0W} = J_W \dot{q} \tag{12}$$

If the shoulder O_S is not constant in the base frame, then J_S is nonzero and we must subtract $J_S \dot{q}$.

Taking the total derivative of (11b), we obtain

$$\dot{\psi} = \frac{1}{\|p_{CE}\|}(e_{SW}^{\times} e_{CE})^T \dot{p}_{CE} - e_y^T \dot{e}_x. \tag{13}$$

Geometrically, these two terms are the angular velocities of p_{CE} and e_x around the axis of rotation e_{SW}. Define J_{f_x} such that $\dot{e}_x = J_{f_x} \dot{p}_{SW}$, which depends on the choice for the function $f_x(p_{SW})$. Then by using (7), we can expand (13) as

$$\dot{\psi} = \frac{1}{\|p_{CE}\|}(e_{SW}^{\times} e_{CE})^T \dot{p}_{0E} - \left(e_y^T J_{f_x} + \frac{e_{SW}^T p_{SE}}{\|p_{SW}\| \, \|p_{CE}\|}(e_{SW}^{\times} e_{CE})^T\right) \dot{p}_{0W} \tag{14}$$

Since we have

$$\dot{\psi} = J_\psi \dot{q} \tag{15}$$

we can write the SEW Jacobian as

$$J_\psi = J_{\psi,E} J_E + J_{\psi,W} J_W, \tag{16}$$

where

$$J_{\psi,E} = \frac{(e_{SW}^{\times} e_{CE})^T}{\|p_{CE}\|}, \tag{17}$$

$$J_{\psi,W} = -e_y^T J_{f_x} - \frac{e_{SW}^T p_{SE}}{\|p_{SW}\| \, \|p_{CE}\|}(e_{SW}^{\times} e_{CE})^T. \tag{18}$$

Table 2
Singularity conditions. Cases 2 and 3 are both algorithmic singularities.

Condition	Singularity Name	Description
1. J loses rank	Kinematic	End effector cannot move in one direction
A. $\mathcal{N}(J)$ tangent to self-motion manifold	Internal	Extra continuous self-motion possible
B. $\mathcal{N}(J)$ not tangent to self-motion manifold	Boundary	Self-motion is instantaneous
2. J_A singular (Full rank J and J_ψ)	Augmentation	Self-motion doesn't change SEW angle
3. J_ψ undefined	SEW Angle	SEW angle undefined
A. O_S, O_E, O_W collinear	Collinear	Depends on choice of O_S, O_E, O_W
B. J_{f_x} undefined	Coordinate	Depends on choice of $f_x(p_{SW})$

We can form the 7×7 augmented Jacobian J_A by stacking J and J_ψ:

$$J_A = \begin{bmatrix} J \\ J_\psi \end{bmatrix}, \quad \begin{bmatrix} \omega \\ v \\ \dot{\psi} \end{bmatrix} = J_A \dot{q}. \tag{19}$$

The augmented task space, which has the end effector orientation as well as the SEW angle, has 7 degrees of freedom.

3.2. Singularity conditions

When controlling a robot using end effector pose augmented with SEW angle, singularities occur when the matrix J_A^{-1} does not exist. When a robot is close to a singularity, there may be large internal joint motion which is undesirable and possibly dangerous, as well as issues with iterative algorithm convergence and numerical precision. Several conditions result in a singularity, as shown in Table 2. Multiple singularity types can occur simultaneously.

The self-motion manifold for 7-DOF spatial manipulators is a curve in joint space for which all points map to the same end effector pose [23]. A single end effector pose may have multiple self-motion manifolds, where each manifold belongs to a different inverse kinematics branch. This manifold exists independently of any parameterization of the redundant degree of freedom, and the goal of parameterizations such as SEW angle is to assign a value to each point on the self-motion manifold. When J is full rank, the self-motion manifold is one-dimensional, and the null space of J, $\mathcal{N}(J)$, is the tangent to the self-motion manifold.

A kinematic singularity occurs when J loses rank, meaning some spatial velocity of the end effector cannot be achieved. This is a condition that depends on the kinematics and joint angles of the robot and does not depend on the parameterization of the redundant degree of freedom. There are two types of kinematic singularities: Internal singularities and boundary singularities. At internal singularities, e.g., when two joint axes are collinear, the null space of J is tangent to the self-motion manifold. A new degree of freedom for self-motion is introduced, but parameterizations such as the SEW angle may not be able to parameterize this degree of freedom. At boundary singularities, e.g., when two links are collinear, the null space of J is not tangent to the self-motion manifold, and self-motion is only instantaneous. In some cases, the entire null space of J causes only instantaneous rather than continuous self-motion, and the self-motion manifold degenerates into a point: The self-motion manifold is zero-dimensional and any parameterization for the redundant degree of freedom is unnecessary because for each inverse kinematics branch, there is only one choice for ψ.

For all conditions other than the kinematic singularity, we call them algorithmic singularities as they occur not because of the robot itself but because of the algorithms we use to parameterize the redundancy. Many authors [24, 67, 68] have defined algorithmic singularities to occur when J_A^{-1} does not exist and J and J_ψ are separately full rank. However, as in [69, 60], we generalize the definition of algorithmic singularity to include cases where J_ψ may not be full rank (i.e., may be a zero vector) or may not exist.

One type of algorithmic singularity is when J_A loses rank, which is possible even when J and J_ψ are full rank. We call this the augmentation singularity, as it occurs only when end effector and SEW angle rates are considered simultaneously. Algebraically, this singularity occurs when J_ψ is linearly dependent with the rows of J. Geometrically, this means self-motion does not cause a change in SEW angle.

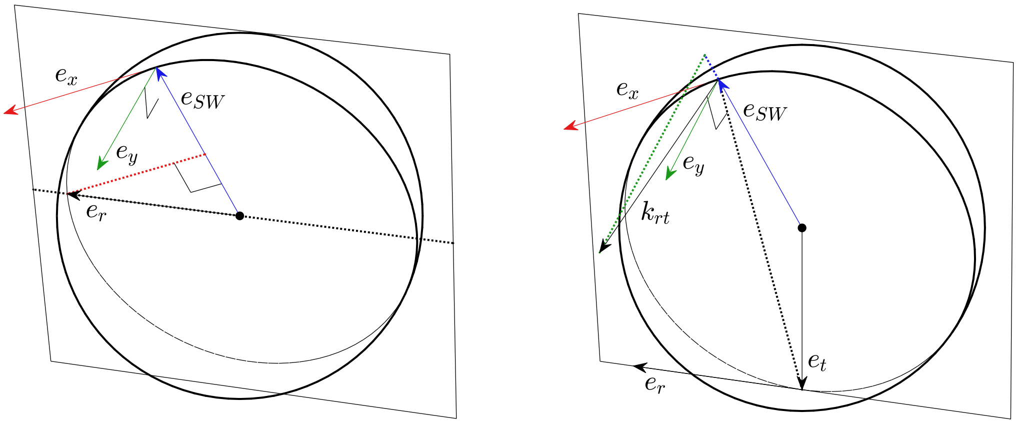

(a) Conventional SEW angle.

(b) Stereographic SEW angle.

Fig. 6. Geometric interpretations for the reference direction function $e_x = f_x(p_{SW})$. (a) In the conventional SEW angle, e_x is the normalized version of the component of e_r orthogonal to the shoulder-wrist direction e_{SW}, and e_y is normal to the plane containing e_{SW} and e_r. (b) In the stereographic SEW angle, k_{rt} is normal to the plane containing $e_{SW} - e_t$ and e_r, e_y is the normalized version of the component of k_{rt} orthogonal to e_{SW}, and e_x is normal to k_{rt} and e_{SW}.

The second type of algorithmic singularity is when J_A^{-1} does not exist because J_ψ does not exist, which we call the SEW angle singularity. There are two cases for the SEW angle singularity. The first case, called the collinear singularity, happens when O_S, O_E, and O_W are collinear, which means $p_{SW} = 0$ or $p_{CE} = 0$. The second case, called the coordinate singularity, is when J_ψ does not exist because J_{f_x} does not exist. In fact, in Section 4, we show that for any choice of $f_x(p_{SW})$ there will always be choices of p_{SW} that cause singularities in J_{f_x}.

Given that the collinear singularity is unavoidable for some robots, it can be beneficial to place O_S, O_E, and O_W such that the SEW angle is undefined exactly when there is only one choice for elbow position per IK branch due to boundary singularities. This reduces the total number of singularities in the workspace. In the case of a 2R-2R-3R robot, placing the shoulder, elbow, and wrist at the joint intersections means that the SEW angle is undefined when the robot has no self-motion of the elbow to parameterize anyway.

The condition of J_ψ losing rank, meaning $J_\psi = 0$, may occur for a general parameterization of the redundant degree of freedom, but for most reasonable choices of placement of O_S, O_E, and O_W, this condition will not occur for the SEW angle. [70] called this case the secondary task singularity.

3.3. *Conventional SEW angle*

The conventional SEW angle, shown in Fig. 6(a), is a widely used parameterization. [24] was the first to provide a detailed analysis of the conventional SEW angle, but the idea was described earlier in [6].

Let e_r be an arbitrary unit reference vector. For the conventional SEW angle, we define the reference direction function f_x as

$$e_x = f_x(p_{SW}) = e_y^\times e_{SW}, \tag{20a}$$

$$e_y = \frac{k_y}{\|k_y\|}, \tag{20b}$$

$$k_y = p_{SW}^\times e_r. \tag{20c}$$

Equivalently, $e_x = f_x(p_{SW})$ is the normalized $-e_{SW}^{\times 2} e_r$, so e_x is the unit vector orthogonal to e_{SW} closest to e_r.

The conventional SEW angle is intuitive to understand. $\psi = 0$ corresponds to the center-elbow direction e_{CE} pointing as much towards e_r as possible. This is similar to navigating on a globe using cardinal directions where e_r provides the north direction and the SEW angle is measured from north.

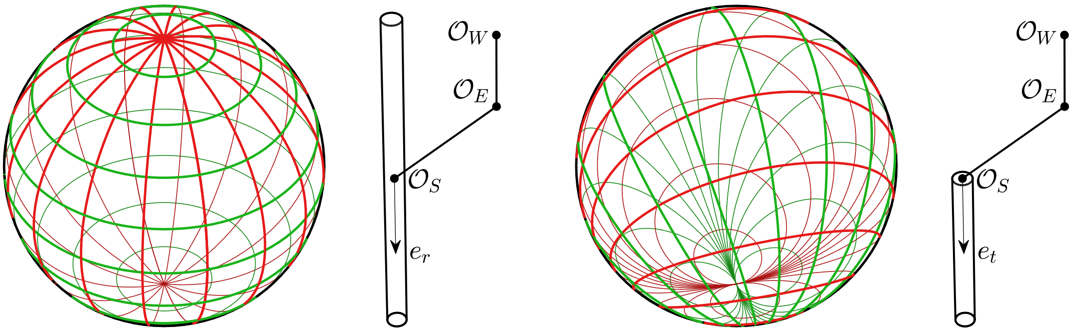

(a) Conventional SEW angle. **(b)** Stereographic SEW angle.

Fig. 7. Grid representing (e_x, e_y) for any choice of shoulder-wrist direction e_{SW} and cylinder representing locations for the wrist O_W where the robot is at or near a coordinate singularity. (a) The conventional SEW angle has two singularities of order one, and the coordinate axes are lines of latitude and longitude. This results in a bidirectional singularity region in task space. (b) The stereographic SEW angle has a single singularity of order 2, which results in a unidirectional singularity region.

The conventional SEW angle becomes undefined and a coordinate singularity occurs when $k_y = p_{SW}^{\times} e_r = 0$, which occurs when p_{SW} is collinear with e_r. In this case. all possible choices of e_{CE} are equally close to e_r. This is akin to being on the north or south pole of a globe where cardinal directions are undefined. If the shoulder is constant in the base frame, then this singularity occurs when the wrist is on the line spanned by e_r passing through the wrist, as shown in Fig. 7(a).

Using the elbow definition of the SEW angle, the conventional SEW angle can be succinctly expressed as

$$\psi = \arg\min_{\theta} \|\mathrm{R}(e_{SW}, \theta) e_r - p_{SE}\|, \tag{21}$$

(notice we may use e_r in place of e_x), which may be directly solved using Subproblem 1 as

$$\psi = \operatorname{atan2}\left((e_{SW}^{\times} e_r)^T p_{SE}, -(e_{SW}^{\times 2} e_r)^T p_{SE}\right) \tag{22a}$$

$$= \operatorname{atan2}(e_{SW}^T e_r^{\times} p_{CE}, e_r^T p_{CE}). \tag{22b}$$

Alternatively, using the plane definition we have

$$\psi = \arg\min_{\theta} \left\|\mathrm{R}(e_{SW}, \theta) k_y - k_{SEW}\right\| \tag{23a}$$

$$= \operatorname{atan2}((e_{SW}^{\times} k_y)^T k_{SEW}, -(e_{SW}^{\times 2} k_y)^T k_{SEW}) \tag{23b}$$

$$= \operatorname{atan2}(e_{SW}^T k_y^{\times} k_{SEW}, k_y^T k_{SEW}). \tag{23c}$$

To calculate the Jacobian, we can express $-e_y^T \dot{e}_x$ as

$$\frac{e_x^T}{\left\|k_y\right\|} \dot{k}_y = \frac{e_x^T}{\left\|k_y\right\|} e_r^{\times} \dot{p}_{SW} = \frac{e_{SW}^T e_r}{\left\|k_y\right\|} e_y^T \dot{p}_{SW}. \tag{24}$$

Therefore, the Jacobian with respect to the wrist is

$$J_{\psi,W} = \frac{e_{SW}^T e_r}{\left\|k_y\right\|} e_y^T - \frac{e_{SW}^T p_{SE}}{\|p_{SW}\| \, \|p_{CE}\|} (e_{SW}^{\times} e_{CE})^T. \tag{25}$$

The Jacobian becomes undefined when $k_y = p_{SW}^{\times} e_r = 0$, again exhibiting the algorithmic singularity condition when e_r and p_{SW} become collinear.

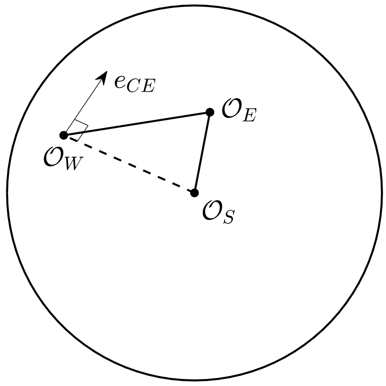

Fig. 8. For each possible position of the wrist O_W on a sphere around the shoulder O_S while fixing the value of the arbitrary redundancy parameterization ϕ, define a unit vector e_{CE} tangent to the sphere and pointing towards the elbow O_E. By the Hairy Ball Theorem, this vector field cannot be continuous.

4. Existence of singularity

[6] showed any revolute manipulator will have internal singularities associated with end effector orientation because it is always possible to find a pose with all joints lying in the same plane. [71] used topology to arrive at the same conclusion: Every smooth map $T^n \rightarrow SO(3)$ must have singularities. Furthermore, he showed it is impossible to construct a smooth left-inverse of a mapping $T^4 \rightarrow SO(3)$, so there is no singularity-free function to map from orientation to joint angles in a 4R joint. (However, it is possible to always find joint angles to follow a given trajectory while avoiding singularities, but this does not follow a function and so will not be cyclical.)

In this section, we will show for a 7-DOF revolute arm with a sufficiently large workspace, e.g., a 3R-R-3R robot with orthogonal consecutive joints, and a task space augmented by any parameterization of the redundant degree of freedom, e.g., the SEW angle, there will always be an algorithmic singularity.

The so-called Hairy Ball Theorem [72] states that a continuous vector field on a sphere must have at least one point where it vanishes. We will use this theorem to show that a singularity must exist for any redundancy parameterization, $\phi : T^7 \rightarrow \mathbb{R}$. Given any end effector pose (R_{0T}, p_{0T}) and ϕ, there exists a finite number of inverse kinematics solutions q. Consider the sphere generated by a constant shoulder-wrist distance $\|p_{SW}\|$ such that the elbow O_E does not lie on the shoulder-wrist line, i.e., p_{SE} and p_{SW} are not collinear. For any point on the sphere and a constant orientation and ϕ, find the inverse kinematics solution q that is on the same branch of the finite number of solutions. Define the vector field $e_{CE}(p_{SE})$ as the unit vector perpendicular to p_{SE} and pointing towards the elbow, which is the normalized version of $-e_{SW}^{\times 2} p_{SE}$, as shown in Fig. 8. By the Hairy Ball Theorem, e_{CE} cannot be continuous everywhere on the sphere. This implies there is a discontinuity in the joint angles while the wrist travels along the sphere, corresponding to the algorithmic singularity.

It is also straightforward to demonstrate that for the general SEW angle specifically, any choice of reference direction function $f_x(p_{SW})$ must have a singularity. If we restrict the input to have some constant nonzero $\|p_{SW}\|$, then f_x defines a unit-magnitude vector field on a sphere. By the Hairy Ball Theorem, this vector field must be discontinuous. For the conventional SEW angle, the singularity occurs when $e_{SW} = \pm e_r$, meaning the shoulder-wrist direction is along the reference direction. If we choose ϕ to be the arm angle where e_x corresponds to the center-elbow direction vector e_{CE} when $q_3 = 0$ and the robot has a spherical wrist, then the singularity occurs when $e_{SW} = \pm h_1$, meaning the shoulder-wrist direction is along the direction of joint axis 1.

Another common parameterization choice is $\phi(q) = q_1$. In this case, if the robot has a spherical wrist then the singularity occurs when $e_{SW} = \pm R_{01} h_2$, meaning the shoulder-wrist direction is along the direction of joint axis 2.

The Poincaré–Hopf theorem [73, 74] implies that not only must there be a singularity on the sphere, but the total order of singularities must be two. For this vector field, the order of the singularity is how many times the elbow rotates about the shoulder-wrist line as the wrist travels around the singularity once. In all the examples of ϕ shown above, there are two antipodal singularities of order one.

The goal of Section 5 is to find a redundancy parameterization that has a single singularity on this sphere of order two. This is in some sense the best-case singularity structure as this results in a singularity along a half-line in the robot workspace. For most robots, this line can be chosen so that it goes into the structure holding the robot in place, meaning the singularity is outside the reachable workspace.

5. Stereographic SEW angle

5.1. Definition

The conventional definition of the SEW angle in Section 3.3 encounters a singularity when the shoulder-wrist vector p_{SW} becomes collinear with the reference vector e_r. As discussed in Section 4, an algorithmic singularity is unavoidable, but we can reduce its impact by slightly changing the SEW angle definition so that the bidirectional line condition becomes a unidirectional half-line condition, as shown in Fig. 7b.

For the stereographic SEW angle (Fig. 6b), we define the reference direction function f_x as

$$e_x = f_x(p_{SW}) = \frac{k_x}{\|k_x\|}, \tag{26a}$$

$$k_x = k_{rt}^{\times} p_{SW}, \tag{26b}$$

$$k_{rt} = (e_{SW} - e_t)^{\times} e_r. \tag{26c}$$

This also means e_y is the normalized version of $-e_{SW}^{\times^2} k_{rt}$. e_t is an arbitrary translation vector chosen to place the singularity structure. We will show we need the conditions $\|e_r\| = 1$, $\|e_t\| = 1$, and $e_r^T e_t = 1$ to achieve the half-line singularity condition. If we instead set $e_t = 0$ then (26) becomes the conventional SEW angle definition.

Using the plane definition, the stereographic SEW angle can be written as

$$\psi = \arg\min_{\theta} \|\mathrm{R}(e_{SW}, \theta) k_{rt} - k_{SEW}\|, \tag{27}$$

(where we recall $k_{SEW} = p_{SW}^{\times} p_{SE}$ is normal to the SEW plane), which may be solved using

$$\psi = \operatorname{atan2}(e_{SW}^T k_{rt}^{\times} k_{SEW}, k_{SEW}^T k_{rt}). \tag{28}$$

Using the elbow definition and recalling $p_{CE} = -e_{SW}^{\times^2} p_{SE}$, we may equivalently write

$$\psi = \operatorname{atan2}(k_{rt}^T p_{CE}, -e_{SW}^T k_{rt}^{\times} p_{CE}). \tag{29}$$

For any (e_r, e_t) with nonzero e_r we can always pick a new $(\tilde{e}_r, \tilde{e}_t)$ such that $e_r^T e_t = 1$ and $\|e_r\| = 1$ where the direction of k_{rt} is identical according to

$$\tilde{e}_r = \frac{e_r}{\|e_r\|}, \quad \tilde{e}_t = -\tilde{e}_r^{\times^2} e_t. \tag{30}$$

We can show that once we require $\|e_r\| = 1$ and $e_r^T e_t = 0$ (without loss of generality), the half-line singularity condition occurs if and only if $\|e_t\| = 1$. The algorithmic singularity corresponds to $k_x = 0$, which occurs when k_{rt} is a zero vector or collinear with e_{SW}. We consider two cases below:

1. $\|e_t\| \leq 1$: For two choices of e_{SW}, $k_{rt} = 0$:

$$e_{SW} = e_t \pm \sqrt{1 - \|e_t\|^2} e_r \tag{31}$$

   This corresponds to the points on the unit sphere that intersect with the line spanned by e_r and translated by e_t.

2. $\|e_t\| \geq 1$: For two choices of e_{SW}, k_{rt} is collinear with e_{SW}:

$$e_{SW} = \frac{e_t}{\|e_t\|^2} \pm \sqrt{\|e_t\|^2 - 1} \frac{e_t^{\times} e_r}{\|e_t\|^2}. \tag{32}$$

   This corresponds to the points on the unit sphere that are tangent to a plane passing through the line spanned by e_r and translated by e_t.

There are two unique singularities if $\|e_t\| < 1$ and two unique singularities if $\|e_t\| > 1$. By choosing $\|e_t\| = 1$, both (31) and (32) simplify to the half-line condition $e_{SW} = e_t$. Geometrically, this is because the line spanned by e_r and translated by e_t only passes through one point on the unit sphere (at e_t), and the only plane tangent to the unit sphere and passing through the line spanned by e_r and translated by e_t is tangent at e_t. If we instead set $e_t = 0$, then we recover the conventional SEW angle as before.

A good choice of e_t is to point in the opposite direction of the robot workspace (e.g., into the ground) so that the singularity will not affect the robot operation.

For the Jacobian, we must calculate

$$-e_y^T \dot{e}_x = -\frac{1}{\|k_x\|} e_y^T \dot{k}_x. \tag{33}$$

Recall that $k_x = k_{rt}^{\times} p_{SW}$, which means the derivative is

$$\dot{k}_x = k_{rt}^{\times} \dot{p}_{SW} - p_{SW}^{\times} \dot{k}_{rt}, \tag{34}$$

and so

$$-e_y^T \dot{e}_x = -\frac{(e_y^{\times} k_{rt})^T}{\|k_x\|} \dot{p}_{SW} + \frac{(e_y^{\times} p_{SW})^T}{\|k_x\|} \dot{k}_{rt}. \tag{35}$$

We can rewrite the first term as

$$-\frac{(e_y^{\times} k_{rt})^T}{\|k_x\|} \dot{p}_{SW} = -\frac{e_{SW}^T k_{rt}}{\|k_x\|} e_x^T J^W \dot{q} = \frac{e_{SW}^T e_t^{\times} e_r}{\|k_x\|} e_x^T J^W \dot{q}. \tag{36}$$

Notice that

$$\dot{e}_{SW} = -\frac{e_{SW}^{\times 2}}{\|p_{SW}\|} \dot{p}_{SW}. \tag{37}$$

The second term can be written as

$$\frac{(e_y^{\times} p_{SW})^T}{\|k_x\|} \dot{k}_{rt} = \frac{\|p_{SW}\|}{\|k_x\|} e_x^T \left(e_r^{\times} \frac{e_{SW}^{\times 2}}{\|p_{SW}\|} J_W \dot{q} \right) = \frac{e_{SW}^T e_r}{\|k_x\|} e_y^T J_W \dot{q}. \tag{38}$$

This means the Jacobian with respect to the wrist is

$$J_{\psi,W} = \frac{e_{SW}^T e_r}{\|k_x\|} e_y^T + \frac{e_{SW}^T e_t^{\times} e_r}{\|k_x\|} e_x^T - \frac{e_{SW}^T p_{SE}}{\|p_{SW}\| \, \|p_{CE}\|} (e_{SW}^{\times} e_{CE})^T \tag{39}$$

As expected based on the previous singularity analysis, other than the $p_{SW} = 0$ and $p_{CE} = 0$ conditions from the general SEW angle, J_ψ is only undefined when $k_x = 0$.

In deriving the Jacobian, we made no assumptions on the norms or orthogonality of e_r or e_t. Setting $e_t = 0$ as before lets us recover the Jacobian for the conventional SEW angle.

5.2. *Relationship to stereographic projection*

The stereographic SEW angle gets its name from stereographic projection, which is a type of one-to-one mapping between points on a sphere and a plane [75]. Stereographic projection has the following geometric definition: Pick a point on the sphere as the pole of the projection and place the plane tangent to the sphere at the antipodal point. Corresponding points on the sphere and plane are collinear with the pole.

We can show the reference direction e_x for the stereographic SEW angle is generated by performing a stereographic projection of a constant vector field onto a unit sphere (Fig. 9). For any choice of unit translation vector e_t and unit reference vector e_r, we can generate a constant vector field in the e_r direction on the projection plane and place the projection pole at e_t. Then, for any choice of shoulder-wrist direction vector e_{SW}, we can form a projection line passing through e_t and e_{SW} and intersecting with the projection plane. The projection of e_r onto the sphere is then the vector that is tangent to the circle formed by the intersection of the unit sphere and the plane that contains the tips of e_t and e_{SW} and is parallel to e_r. This plane is normal to $k_{rt} = (e_{SW} - e_t)^{\times} e_r$, and so the projection of e_r from the plane to the sphere is e_x.

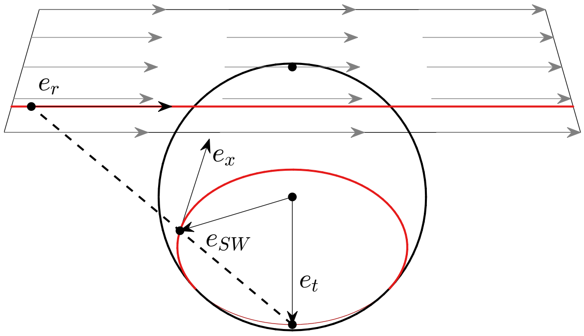

Fig. 9. The stereographic projection of the unit reference vector e_r onto the shoulder-wrist direction vector e_{SW} is e_x, where the pole of the projection is at the unit translation vector e_t.

5.3. Preservation of angles

Although it appears that we have three DOF in picking the parameters for the stereographic SEW angle (two DOF for the unit translation vector e_t and one remaining DOF for the unit reference vector e_r), we can show that the one DOF for e_r does not change the behavior of the SEW angle; it only changes the angle by a constant. Changing the angle of e_r around e_t is equivalent to changing the SEW angle ψ by the same angle.

Since stereographic projection is a conformal mapping, changes of angles in the projection plane get preserved after projecting onto the unit sphere. This means changing the angle of e_r on the projection plane corresponds to an equal change of angle to e_x and e_y.

We can also prove this preservation of angles property directly (Fig. 10). First, set $e_r = e_{r,1}$, which results in $e_{x,1}$. This vector is tangent to the circle that is tangent to $e_{r,1}$ and passes through the shoulder-wrist direction vector e_{SW} and e_t. Now, pick a new $e_r = e_{r,2}$ that is $e_{r,1}$ rotated by an angle α about $-e_t$. This generates $e_{x,2}$ which is tangent to the circle passing through e_{SW} and e_t but tangent to $e_{r,2}$. The angle from $e_{x,1}$ to $e_{x,2}$ about e_{SW} is an angle β. The angles of intersection of any two circles on a sphere are equal, so $\alpha = \beta$.

The preservation of angles property can aid in analyzing the behavior of the SEW angle when only q_1 changes in the typical case of $e_t = -h_1$, which occurs when the first joint axis of the robot points up and the singularity direction is chosen to point down. In this case, when q_1 changes but all other joint angles are held constant, ψ changes at the same rate. This means the first element of the SEW angle Jacobian J_ψ is always 1.

We can compare this to the conventional SEW angle where $e_r = h_1$. In this case, the SEW angle does not change when only q_1 changes. (The conventional SEW angle has rotational invariance about e_r.) This means the first element of J_ψ is always 0.

5.4. Singularity behavior

The singularity for the stereographic SEW angle is of order two. This means that if e_{SW} travels in a small circle around e_t, e_x rotates twice for each rotation of e_{SW}. This is unlike the conventional SEW angle, where each singularity is of order one.

Although a singularity of order two would result in larger elbow motion than a singularity of order one for a fixed SEW angle as e_{SW} passes close to e_t, large motion disappears if e_{SW} passes directly through e_t in a smooth path. As a path gets closer to the singularity, e_x gets closer to making a full revolution of 2π radians. At the limit, the elbow rotates by exactly 2π, which is equivalent to not rotating at all. We can compare this to the conventional SEW angle, where passing through the singularity in a smooth path causes e_x to rotate by π radians.

5.5. Comparison demonstration

Two joint trajectories were generated for a KUKA LBR iiwa 14 R820 robot [36] with constants $R_{07} = I$ and $\psi = \pi/4$: One using the conventional SEW angle with $e_r = [0\ 0\ 1]^T$, and the other using the stereographic SEW angle with $e_t = [0\ 0\ -1]^T$ and $e_r = [0\ 1\ 0]^T$. The task-space trajectory for p_{0T} took a straight-line path through four points, with $x = \pm 0.40$ m, $y = 0.01$ m, and $z = 0.36 \pm 0.40$ m. There was a small offset in the y direction as otherwise there

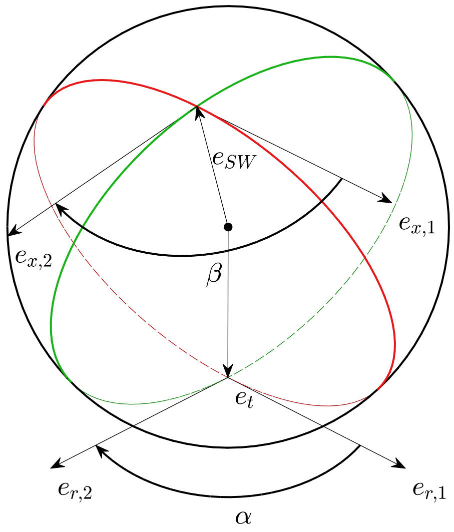

Fig. 10. $e_{x,i}$ is tangent to the circle generated from the plane through e_t, $e_t + e_{r,i}$ and e_{SW}. The angles of intersection of any two circles on a sphere are equal. Therefore, $\alpha = \beta$.

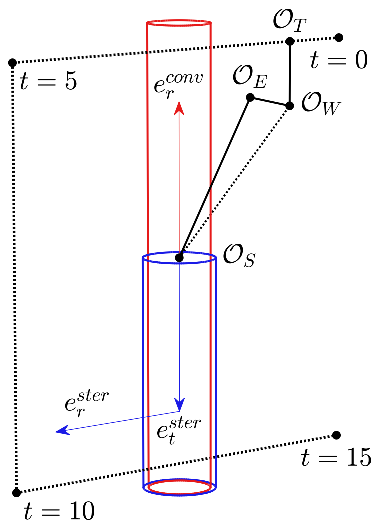

Fig. 11. Task-space trajectory for the comparison demonstration. The end effector position follows three line segments while the end effector rotation and SEW angle are constant. The red and blue cylinders indicate the conventional and stereographic SEW angle singularity directions, respectively.

would not be any large joint motion for the stereographic SEW angle. For each trajectory, the initial pose was picked such that $q_2 > 0$, $q_4 > 0$, and $q_6 > 0$. The task-space trajectory is shown in Fig. 11, and the results are shown in Fig. 12 (Extension 1).

For the conventional SEW angle, the singularities occur near $e_{SW} = \pm[0\ 0\ 1]^T$. In following the trajectory with the conventional SEW angle, there were large joint motions in two places, each corresponding to the positive and negative direction.

For the stereographic SEW angle, the singularity only occurs near $e_{SW} = [0\ 0\ {-1}]^T$. We see that the large joint motion only occurred at one time in the trajectory. The joint motion was also larger than in the conventional SEW case, as the singularity is of order two instead of one. The singularity occurs when the wrist is below the base, which in many cases would be out of the feasible workspace.

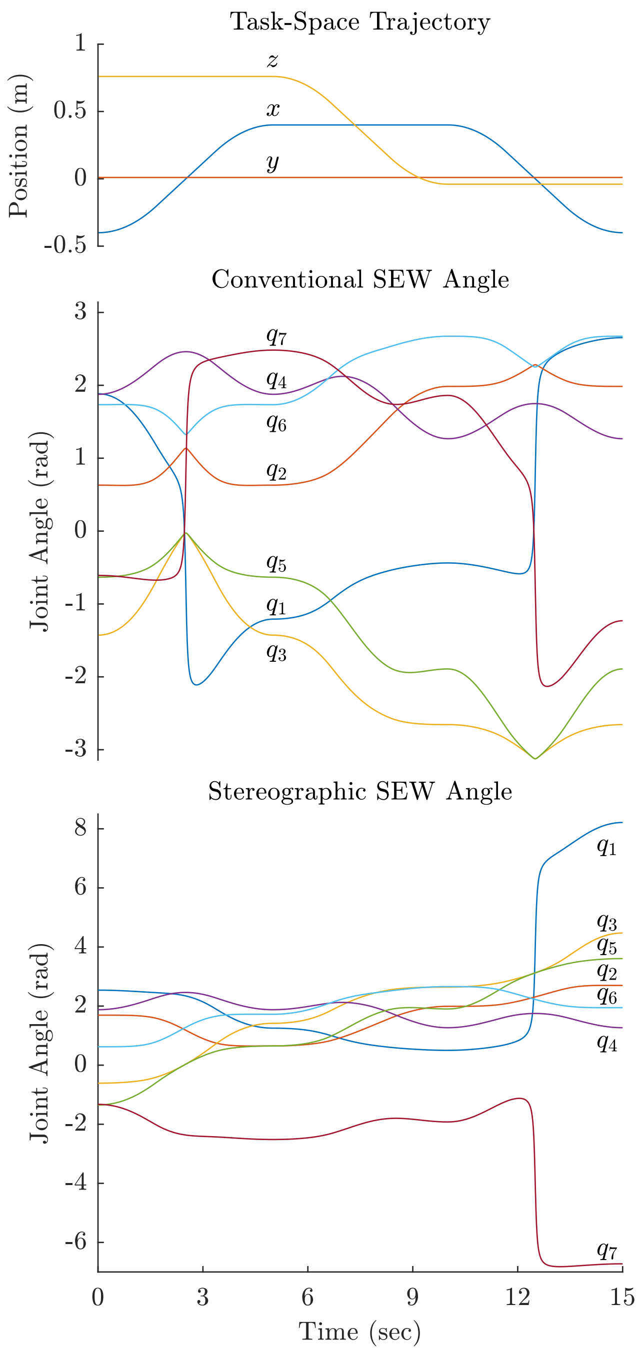

Fig. 12. Joint-space trajectories using constant conventional or stereographic SEW angles. Whereas the conventional SEW angle results in large joint motion when the wrist passes near a line, the stereographic SEW angle results in large joint motion when passing near a half-line. This unidirectional singularity region occurs below the robot ($z < 0$) and cannot typically be reached. (See also Extension 1.)

Table 3
Kinematic families of robots with IK solutions demonstrated in this paper. The Motoman SIA50D appears as two examples since one robot may be part of multiple kinematic families.

IK Type	Kinematic Family	Robot Example
Closed-Form	1. 2R-2R-3R	FREND (OSAM-1)[76]
		KUKA LBR iiwa 14 R820 [36]
	2. 3R-R-3R	Motoman SIA5D [35]
	3. R-R-3R^{E}-2R	Motoman SIA50D [14]
	4. 2R-3R-2R	
	5. 2R-3R‖-2R	SSRMS [5]
		SPDM [77]
		ERA [78]
	6. R-R-3R‖^{E}-2R	
1D Search	7. R-2R-2R^{E}-2R	Sawyer [3]
		Baxter [2]
		xLink (OSAM-2) [79]
		OB7 [80]
	8. 3R-R^{E}-2R-R	Franka Production 3 [81]
		xArm7 [82]
	9. R-2R^{S}-R-3R	Motoman SIA50D [14]
2D Search	10. General 7-DOF	ABB YuMi [4]
		RRC [1]

6. Inverse kinematics

6.1. Problem formulation

The inverse kinematics problem for a 7R robot arm is to find all possible joint angles q corresponding to an end effector pose and SEW angle (R_{0T}, p_{0T}, ψ) given the robot kinematic parameters $\left(\{p_{i-1,i}\}_{i=1}^{7},\ p_{7T},\ \{h_i\}_{i=0}^{7},\ R_{7T}\right)$ and stereographic SEW parameters $\left(e_r,\ e_t,\ p_{iS},\ p_{jE},\ p_{kW}\right)$. These inverse kinematics solutions are agnostic to the SEW formulation, and so the conventional SEW angle definition may be used instead.

The inverse kinematics procedures can apply not just to 7-DOF manipulators, but also to 6-DOF manipulators that have been provided an extra degree of freedom, say, by being placed on an omnidirectional mobile base with the location of the origin of the base specified. For example, if we use a UR5 robot [83], tilt the robot so the first joint is not vertical, and pick the origin of the mobile base to be directly under the intersection of joints 1 and 2, then the system becomes a 3R-R-2R-R or 3R-2R‖-2R robot.

To find the inverse kinematics of a 7-DOF robot where the redundant degree of freedom is parameterized by some joint angle q_i, find the 6-DOF robot generated by fixing q_i and refer to the inverse kinematics procedures provided in [20].

Without loss of generality, assume $p_{01} = 0$, meaning the origin of joint 1 is coincident with the base frame origin. (Otherwise, subtract p_{01} from the end effector position p_{0T} and the shoulder position p_{0S}.) Rewrite the kinematics equations in terms of R_{07} and p_{07}, which are the pose of the 7 frame and can be immediately calculated:

$$R_{07} = R_{0T}R_{7T}^{T} = R_{01}R_{12}R_{23}R_{34}R_{45}R_{56}R_{67}, \tag{40a}$$

$$p_{07} = p_{0T} - R_{07}p_{7T} = R_{01}p_{12} + R_{02}p_{23} + R_{03}p_{34} + R_{04}p_{45} + R_{05}p_{56} + R_{06}p_{67}. \tag{40b}$$

The inverse kinematics procedures can now be written in terms of $(R_{07},\ p_{07},\ \psi)$. If the shoulder is constant in the 0 frame and the wrist is constant in the 7 frame, then we can use (9) to find n_{SEW} since ψ is given and p_{SW} is known:

$$p_{SW} = p_{07} + R_{07}p_{7W} - p_{0S}. \tag{41}$$

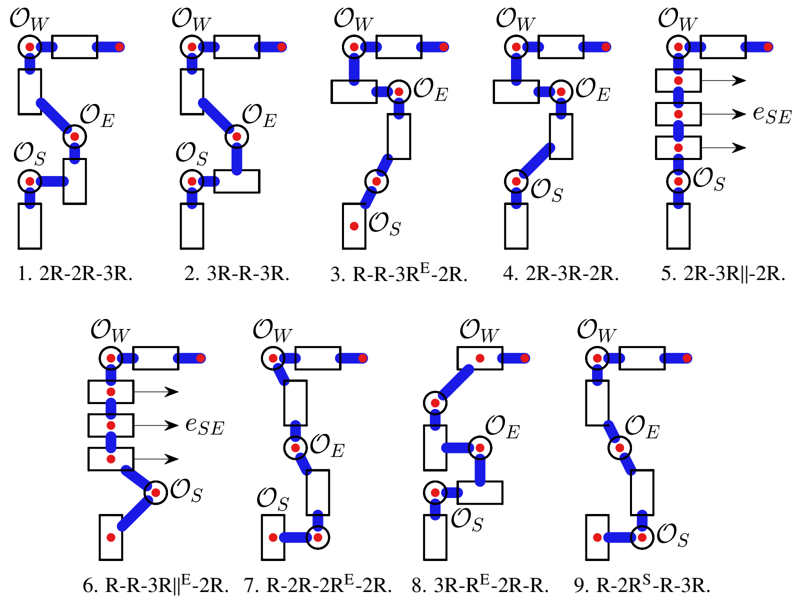

Fig. 13. Examples of robots in kinematic families with closed-form and 1D search solutions.

A key step in the inverse kinematics procedure is to find the elbow location, i.e., p_{SE}. This sometimes involves finding the shoulder angle θ_S or the wrist angle θ_W, defined as

$$p_{SE} = \mathrm{R}(n_{SEW}, \theta_S) e_{SW} \, \|p_{SE}\| \,, \tag{42}$$

$$p_{EW} = \mathrm{R}(n_{SEW}, \theta_W) e_{SW} \, \|p_{EW}\| \,. \tag{43}$$

Note that for a given shoulder position, wrist position, and SEW angle, the elbow must be somewhere in a half-plane: Given the SEW plane normal vector n_{SEW} and center-elbow direction vector e_{CE}, we require $n_{SEW}^T p_{SE} = 0$ and $e_{CE}^T p_{SE} > 0$. To place the elbow in the correct half-plane, $\theta_S \in [0, \pi]$ and $\theta_W \in [-\pi, 0]$. A singularity occurs when $\theta_S = 0$ or $\theta_W = 0$, as this corresponds to the shoulder, elbow, and wrist being collinear.

Several inverse kinematics solutions based on the subproblem decomposition method presented in [20] are provided below, and the different kinematic families along with some specific robot examples are shown in Table 3 and Fig. 13. There exist many other kinematic families, but we include enough examples to demonstrate the technique of applying the subproblem decomposition method to solve the inverse kinematics problem. The reader is referred to the discussions in [20] for information regarding handling multiple branches, extraneous solutions, least-squares solutions, 1D and 2D searches, and internal and boundary singularities.

Closed-form solutions may exist when a robot has 3R or 3R|| joints, as a 3R joint may result in decoupling between position and orientation, and a 3R|| joint is the limit of a 3R joint as the point of intersection moves infinitely far away. (It only makes sense to place O_E infinitely far away, as placing O_S or O_W infinitely far away results in the shoulder-wrist direction e_{SW} being a constant vector in the base or end effector frame.) In other cases, the solution requires a 1D or 2D search over q_i, θ_S, or θ_W. We also demonstrate converting a search-based solution into a polynomial root-finding problem using the tangent half-angle substitution in Section 6.4.

A common step in the IK solutions below is to solve the orientation of a 3R joint. To solve such a spherical joint (shown here at the robot wrist)

$$R_{45} R_{56} R_{67} = R_{47}, \tag{44}$$

first solve for (q_5, q_6) using Subproblem 2:

$$R_{56} h_7 = R_{54} R_{47} h_7. \tag{45}$$

Then, solve for q_7 using Subproblem 1:

$$R_{67} p = R_{65} R_{54} R_{47} p, \tag{46}$$

where p is any vector not collinear with h_7.

In the following IK solutions, always pick the origins of intersecting axes for that kinematic family to be coincident. For example, in a 3R-R-3R robot, pick $O_1 = O_2 = O_3 = O_S$, which means $p_{12} = p_{23} = p_{0S} = 0$. When an elbow is made of parallel joints (say, that include joint 3), pick $p_{SE} = e_{SE} = R_{02}h_3$ so the shoulder-elbow direction is equal to the third joint axis.

6.2. *IK solutions*

6.2.1. *2R-2R-3R arm*

The position equation becomes

$$p_{07} = p_{SW} = R_{02}(p_{23} + R_{24}p_{45}), \tag{47}$$

and given θ_S we have

$$R_{02}p_{23} = \mathrm{R}(n_{SEW}, \theta_S)e_{SW}\,\|p_{23}\|\,. \tag{48}$$

Use Subproblem 3 to find $\theta_S \in [0, \pi]$:

$$\|\mathrm{R}(n_{SEW}, \theta_S)e_{SW}\,\|p_{23}\| - p_{07}\| = \|p_{45}\|\,. \tag{49}$$

Find (q_1, q_2) using Subproblem 2:

$$R_{12}p_{23} = R_{10}\mathrm{R}(n_{SEW}, \theta_S)e_{SW}\,\|p_{23}\|\,. \tag{50}$$

Similarly, find (q_3, q_4) using Subproblem 2:

$$R_{32}(R_{21}R_{10}p_{07} - p_{24}) = R_{34}p_{45}. \tag{51}$$

Finally, find (q_5, q_6, q_7) by solving the spherical wrist:

$$R_{45}R_{56}R_{67} = (R_{01}R_{12}R_{23}R_{34})^T R_{07}. \tag{52}$$

6.2.2. *3R-R-3R arm*

The position equation becomes

$$p_{07} = p_{SW} = R_{03}(p_{34} + R_{34}p_{45}). \tag{53}$$

Solve for up to two solutions of q_4 using Subproblem 3:

$$\|R_{34}p_{45} + p_{34}\| = \|p_{07}\|\,. \tag{54}$$

Represent R_{03} as three consecutive orthogonal rotations:

$$R_{03} = \mathrm{R}(e_{SW}, \theta_a)\mathrm{R}(n_{SEW}, \theta_b)\mathrm{R}(e_{SW}, \theta_c). \tag{55}$$

There are up to two solutions for $(\theta_a, \theta_b, \theta_c)$, but they represent the same R_{03}, so only keep one solution. Solve for (θ_b, θ_c) using Subproblem 2:

$$\mathrm{R}(n_{SEW}, \theta_b)^T p_{07} = \mathrm{R}(e_{SW}, \theta_c)(p_{34} + R_{34}p_{45}). \tag{56}$$

Then, use Subproblem 4 to find θ_a, keeping only the solutions that place the elbow in the correct half-plane:

$$n_{SEW}^T\mathrm{R}(e_{SW}, \theta_a)\mathrm{R}(n_{SEW}, \theta_b)\mathrm{R}(e_{SW}, \theta_c)p_{3E} = 0. \tag{57}$$

Find (q_1, q_2, q_3) by solving the spherical shoulder:

$$R_{01}R_{12}R_{23} = \mathrm{R}(e_{SW}, \theta_a)\mathrm{R}(n_{SEW}, \theta_b)\mathrm{R}(e_{SW}, \theta_c). \tag{58}$$

Similarly, find (q_5, q_6, q_7) by solving (52).

6.2.3. R-R-3R^E-2R arm

Write θ_W as

$$R_{05}p_{56} = \mathrm{R}(n_{SEW}, \theta_W)e_{SW}\,\|p_{56}\|\,. \tag{59}$$

Using Subproblem 5, we can find up to four solutions of (q_1, q_2, θ_W), where $\theta_W \in [-\pi, 0]$:

$$p_{07} - \mathrm{R}(n_{SEW}, \theta_W)e_{SW}\,\|p_{56}\| = R_{01}(p_{12} + R_{12}p_{23}). \tag{60}$$

Next, find up to two solutions of (q_6, q_7) using Subproblem 2:

$$R_{67}R_{07}^T\mathrm{R}(n_{SEW}, \theta_W)e_{SW}\,\|p_{56}\| = R_{65}p_{56}. \tag{61}$$

To solve for (q_3, q_4, q_5), solve the spherical elbow:

$$R_{23}R_{34}R_{45} = (R_{01}R_{12})^T R_{07}(R_{56}R_{67})^T. \tag{62}$$

6.2.4. 2R-3R-2R arm

Find $\theta_S \in [0, \pi]$ using Subproblem 3:

$$\|\mathrm{R}(n_{SEW}, \theta_S)e_{SW}\,\|p_{23}\| - p_{07}\| = \|p_{56}\|\,. \tag{63}$$

Find (q_1, q_2) with Subproblem 2 to solve (50). Similarly, find (q_6, q_7):

$$R_{67}R_{07}^T(p_{07} - R_{02}p_{23}) = R_{65}p_{56}. \tag{64}$$

Find (q_3, q_4, q_5) by solving (62).

6.2.5. 2R-3R‖-2R arm

This robot is the limit of a 2R-3R-2R arm where the intersection point of the elbow joint moves to infinity. We can write

$$R_{01}R_{12}h_3 = \mathrm{R}(n_{SEW}, \theta_S)e_{SW}. \tag{65}$$

Combining with the position equation gives

$$h_3^T(p_{23} + p_{34} + p_{45} + p_{56}) = h_3^T R_{02}^T p_{07}. \tag{66}$$

Solve for $\theta_S \in [0, \pi]$ using Subproblem 4:

$$e_{SW}^T\mathrm{R}(n_{SEW}, \theta_S)^T p_{07} = h_3^T(p_{23} + p_{34} + p_{45} + p_{56}). \tag{67}$$

Find (q_1, q_2) using Subproblem 2:

$$R_{12}h_3 = R_{10}\mathrm{R}(n_{SEW}, \theta_S)e_{SW}. \tag{68}$$

Find $(q_3 + q_4 + q_5, q_6, q_7)$ by solving a spherical joint:

$$R_{25}R_{56}R_{67} = R_{02}^T R_{07}. \tag{69}$$

Use Subproblem 3 to find q_4:

$$\|p_{34} + R_{34}p_{45}\| = \left\|R_{02}^T p_{07} - p_{23} - R_{25}p_{56}\right\|. \tag{70}$$

Use Subproblem 1 to find q_3:

$$R_{23}(p_{34} + R_{34}p_{45}) = R_{02}^T p_{07} - p_{23} - R_{25}p_{56}. \tag{71}$$

Find q_5 with subtraction, wrapping to $[-\pi, \pi]$ if desired.

6.2.6. R-R-3R$\|^E$-2R arm

This is a more general version of a 2R-3R‖-2R robot. Use Subproblem 6 to find (θ_S, q_2), where $\theta_S \in [0, \pi]$:

$$e_{SW}^T \mathrm{R}(n_{SEW}, \theta_S)^T p_{07} - h_3^T R_{21} p_{12} = h_3^T (p_{23} + p_{34} + p_{45} + p_{56}), \tag{72a}$$

$$h_1^T \mathrm{R}(n_{SEW}, \theta_S)\, e_{SW} - h_1^T R_{12} h_3 = 0. \tag{72b}$$

Use Subproblem 1 to find q_1 solving (65). Find $(q_3+q_4+q_5, q_6, q_7)$ by solving a spherical joint (69). Use Subproblem 3 to find q_4:

$$\|p_{34} + R_{34} p_{45}\| = \left\| R_{02}^T p_{07} - R_{21} p_{12} - p_{23} - R_{25} p_{56} \right\|. \tag{73}$$

Use Subproblem 1 to find q_3:

$$R_{23}(p_{34} + R_{34} p_{45}) = R_{02}^T p_{07} - R_{21} p_{12} - p_{23} - R_{25} p_{56}. \tag{74}$$

Find q_5 with subtraction, wrapping to $[-\pi, \pi]$ if desired.

6.2.7. R-2R-2R^E-2R arm (1D search)

Given θ_W, we can write

$$R_{05} p_{56} = \mathrm{R}(n_{SEW}, \theta_W) e_{SW} \|p_{56}\|. \tag{75}$$

Then, find q_1 using Subproblem 3:

$$\|R_{01} p_{12} - p_{07} + R_{05} p_{56}\| = \|p_{34}\|. \tag{76}$$

Find (q_2, q_3) using Subproblem 2:

$$R_{23} p_{34} = R_{21}(R_{10} p_{07} - R_{10} R_{05} p_{56} - p_{12}). \tag{77}$$

Find (q_4, q_5) using Subproblem 2:

$$R_{45} p_{56} = R_{43}(R_{32} R_{21}(R_{10} p_{07} - p_{12}) - p_{34}). \tag{78}$$

The error is a metric of the solvability of

$$R_{56} R_{67} = R_{05}^T R_{07}. \tag{79}$$

By projecting onto h_6 and h_7, we get the error

$$e(\theta_W) = h_6^T R_{05}^T R_{07} h_7 - h_6^T h_7. \tag{80}$$

Search over $\theta_W \in [-\pi, 0]$ to find all solutions of $e(\theta_W) = 0$. For each solution θ_W, calculate q_6 and q_7 using Subproblem 1:

$$R_{56} h_7 = R_{05}^T R_{07} h_7, \tag{81}$$

$$R_{76} h_6 = R_{07}^T R_{05} h_6. \tag{82}$$

A Sawyer arm example is shown in Fig. 14 and Fig. 15 (Extension 2).

6.2.8. 3R-R^E-2R-R arm (1D search)

Given $\theta_S \in [0, \pi]$, we have

$$R_{03} p_{34} = \mathrm{R}(n_{SEW}, \theta_S) e_{SW} \|p_{34}\|. \tag{83}$$

Use Subproblem 3 to find q_7 from

$$\left\| R_{07}^T (p_{07} - R_{03} p_{34}) - R_{76} p_{67} \right\| = \|p_{45}\|. \tag{84}$$

Then, solve (q_5, q_6) using Subproblem 2:

$$R_{54} p_{45} = R_{56}(R_{67} R_{07}^T (p_{07} - R_{03} p_{34}) - p_{67}). \tag{85}$$

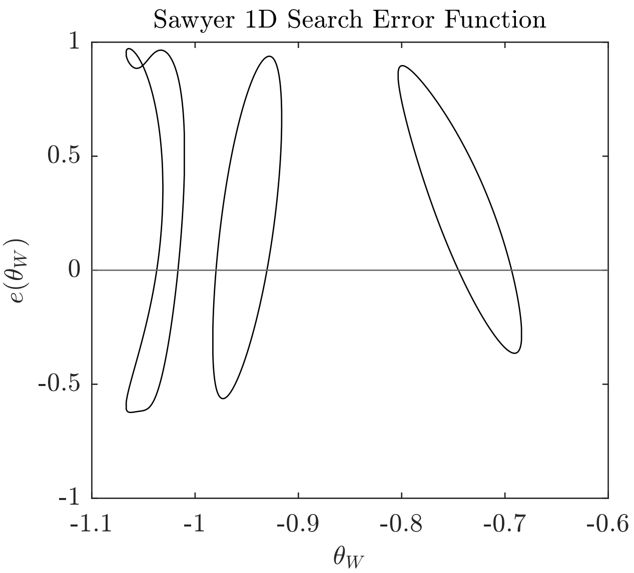

Fig. 14. Error function for a Sawyer (R-2R-2R$^{\mathrm{E}}$-2R) arm. This function has eight branches, although only four are seen for this pose. A 1D search may be used to find the zeros, which correspond to IK solutions.

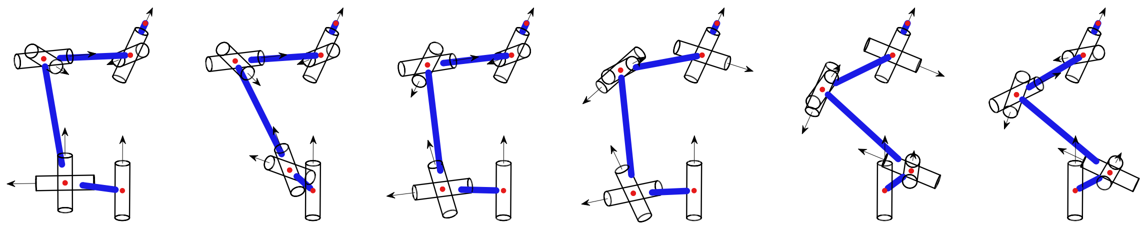

(a) $\theta_W = -1.0371$. **(b)** $\theta_W = -1.0166$. **(c)** $\theta_W = -0.9797$. **(d)** $\theta_W = -0.9304$. **(e)** $\theta_W = -0.7450$. **(f)** $\theta_W = -0.6936$.

Fig. 15. Six IK solutions for a Sawyer (R-2R-2R$^{\mathrm{E}}$-2R) arm corresponding to the zeros of the error shown in Fig. 14.

We have the identity

$$R_{43}p_{34} = R_{47}R_{07}^T R_{03}p_{34}, \tag{86}$$

which may be expressed as an error function in terms of θ_S:

$$e(\theta_S) = h_4^T(p_{34} - R_{47}R_{07}^T R_{03}p_{34}). \tag{87}$$

Search over $\theta_S \in [0, \pi]$ to find the zeros of this error. For each solution θ_S, find q_4 with Subproblem 1, then find (q_1, q_2, q_3) by solving the spherical shoulder:

$$R_{01}R_{12}R_{23} = R_{07}(R_{34}R_{45}R_{56}R_{67})^T. \tag{88}$$

6.2.9. R-2R^S-R-3R arm (1D search)

Given $q_1 \in [-\pi, \pi]$, solve for q_4 using Subproblem 3:

$$\|p_{34} + R_{34}p_{45}\| = \|R_{10}p_{07} - p_{12}\|. \tag{89}$$

Solve for (q_2, q_3) using Subproblem 2:

$$R_{21}(R_{10}p_{07} - p_{12}) = R_{23}(p_{34} + R_{34}p_{45}). \tag{90}$$

Find the shoulder-elbow vector $p_{SE} = R_{03} p_{34}$, from which we can calculate the error for ψ in terms of q_1. A plot of this error is a good graphical tool to determine what range of SEW angle is feasible for a given end effector pose. For each solution q_1, find (q_5, q_6, q_7) by solving (52).

6.2.10. General 7-DOF arm (2D search)

Pick $O_1 = O_S$, $O_4 = O_E$, and $O_7 = O_W$. The shoulder, elbow, and wrist may be placed arbitrarily as in Fig. 3 and the solution will remain similar. Given (q_1, q_2), find q_3 using Subproblem 4, keeping only solutions that place the elbow in the correct half-plane:

$$n_{SEW}^T R_{02} R_{23} p_{34} = -n_{SEW}^T (R_{01} p_{12} + R_{02} p_{23}). \tag{91}$$

Then, find (q_5, q_6, q_7) with Subproblem 5 to solve

$$-p_{67} + R_{67} R_{07}^T (p_{07} - p_{14}) = R_{65} (p_{56} + R_{54} p_{45}), \tag{92}$$

and find the error

$$e(q_1, q_2) = \left\| R_{03}^T R_{07} R_{47}^T h_4 - h_4 \right\|. \tag{93}$$

Search over (q_1, q_2) to find zeros of this error. Then, find q_4 using Subproblem 1:

$$R_{34} p = R_{03}^T R_{07} R_{47}^T p, \tag{94}$$

where p is any vector not collinear with h_4.

6.3. Continuous and least-squares IK

Using the subproblem decomposition approach means that continuous non-exact solutions for q are returned even for branches where the solution does not exist, as discussed in [20]. Therefore, IK is numerically stable for paths where the robot switches branches by passing through a boundary singularity.

For some special cases, the IK solution is also the solution to the global least-squares IK problem, which is posed as

$$\min_q \left\| p_{0T}(q) - p_{0T}^{des} \right\| \text{ s.t. } R_{0T}(q) = R_{0T}^{des},\ \psi(q) = \psi^{des} \tag{95}$$

where $(R_{0T}^{des}, p_{0T}^{des}, \psi^{des})$ is the desired end effector pose and SEW angle. For some robots, the $\psi(q) = \psi^{des}$ constraint cannot be achieved when at a boundary singularity because the self-motion manifold degenerates to a point, and so this constraint must be dropped when $p_{0T}(q) \neq p_{0T}^{des}$.

3R-R-3R, 2R-3R-2R, and 2R-2R-3R arms can all achieve least-squares inverse kinematics if the task frame is at the wrist center ($p_{7T} = 0$), all 2R joints have a spherical workspace ($h_i^T h_{i+1} = h_{i+1}^T p_{i+1,i+2} = 0$) and all 3R joints can achieve any orientation ($h_i^T h_{i+1} = h_{i+1}^T h_{i+2} = 0$).

For a 3R-R-3R arm, since a rotation of the whole arm is always possible between the spherical shoulder and wrist, the self-motion manifold does not degenerate to a point at boundary singularities. Therefore, O_E should be placed such that it is not collinear with O_S and O_W at the workspace boundary. (Using $p_{SE} = e_{SE} = R_{03} h_4$ may also be a good option.)

For 2R-3R-2R and 2R-2R-3R arms, the robot's self-motion manifold degenerates into a point at boundary singularities, so although the SEW angle will be undefined at the boundary singularity, the SEW angle is not needed. This also means the SEW angle constraint in (95) must be dropped.

6.4. Polynomial method

The tangent half-angle substitution $x_i = \tan(q_i/2)$ can be used to convert a search-based solution into a system of multivariate polynomials. By eliminating all but one variable, we obtain a high-order polynomial in the tangent half-angle of one joint. After finding the roots of this polynomial, the remaining joint angles are found in closed form. Although this procedure is not as computationally efficient as 1D or 2D search, it does give a stronger guarantee of finding all solutions. We demonstrate solving IK using the polynomial method for the Sawyer (R-2R-2R$^{\mathrm{E}}$-2R) arm according to the procedure described in [20].

To improve computational performance, we reduce the number of variables and search over a joint angle rather than θ_W. The downside is that we must check for extraneous solutions where the elbow is in the wrong half-plane.

Table 4
Sawyer IK solutions using the polynomial method.

#	q_1	q_2	q_3	q_4	q_5	q_6	q_7
1	0.7012115792	-0.9732888736	-0.09318675442	1.466219046	1.023549438	-0.7523604269	-0.8108011807
2	-1.187806104	-2.406581118	2.111970078	1.816987670	1.723460652	-0.7764631130	-0.7042361521
3	-0.4801904691	-1.230875621	-2.301720627	-2.019222054	-2.695866355	-0.8165545740	-0.5807494539
4	-2.104051752	-2.319400366	-0.7687046831	-0.5435788511	2.572212359	0.7314410389	0.9764868428
5	0.7028860908	-1.034458755	0.05293672172	0.9219195962	-1.476315039	0.7522268563	1.404840771
6	-1.439122724	-2.605604387	1.821941574	0.9918815495	-0.4713994287	0.7552919261	1.423570856
7	-0.2361394798	-1.013327345	-2.064532180	-1.375427168	1.007651470	0.8154933152	1.682578759

Given q_7, find q_6 using Subproblem 4:

$$(R_{67}R_{07}^T n_{SEW})^T R_{65} p_{56} = n_{SEW}^T p_{07}. \tag{96}$$

Then, find q_1 with Subproblem 3 according to (76), where $R_{05} = R_{07}R_{76}R_{65}$. Although Subproblem 2 could be used to find q_2 and q_3 using (77), we instead first solve for q_2 with Subproblem 4 to solve

$$h_3^T R_{21}(R_{10}p_{07} - R_{10}R_{05}p_{56} - p_{12}) = h_3^T p_{34}, \tag{97}$$

and then find q_3 with Subproblem 1. This allows us to eliminate x_3 from the system of polynomials. The error is

$$e(q_7) = h_4^T R_{03}^T R_{07} R_{57}^T h_5 - h_4^T h_5. \tag{98}$$

For all solutions of $e(q_7) = 0$, we can find q_4 and q_5 with Subproblem 1:

$$R_{34}h_5 = R_{03}^T R_{07} R_{57}^T h_5, \tag{99}$$
$$R_{54}h_4 = R_{57}R_{07}^T R_{03} h_4. \tag{100}$$

The Sawyer kinematics parameters (in mm) are:

$$\begin{gathered} h_1 = [0\ 0\ 1]^T, \quad h_2 = h_4 = h_6 = [0\ 1\ 0]^T, h_3 = h_5 = h_7 = [1\ 0\ 0]^T, \\ p_{12} = [81\ 192.5\ 0]^T,\ p_{23} = p_{45} = p_{67} = 0, p_{34} = [400\ {-168.5}\ 0]^T,\ p_{56} = [400\ 136.3\ 0]^T. \end{gathered} \tag{101}$$

Using the conventional SEW angle, we pick the following example pose (in mm):

$$R_{06} = I_3, \quad p_{06} = [500\ 500\ 250]^T, \quad \psi = 0, \quad e_r = [0\ 0\ 1]^T. \tag{102}$$

The stereographic SEW angle can be used just as easily since the solution only depends on n_{SEW}.

After converting all subproblems and the error equation using the tangent half-angle identity, we find four equations in four unknowns with $(23, 42, 5, 291)$ terms, respectively:

$$P_1(x_1, x_6, x_7) = 0, \quad P_2(x_1, x_2, x_6, x_7) = 0, \quad P_3(x_6, x_7) = 0, \quad P_4(x_1, x_2, x_6, x_7) = 0. \tag{103}$$

Eliminating all variables but x_7, we find a resultant univariate polynomial of degree 48. Of the 16 real solutions, 7 correspond to solutions to the IK problem, and the other 9 solutions correspond to poses with $\psi = \pi$. All 7 IK solutions for this pose are shown in Table 4 to 10 significant figures.

7. Conclusion

We have introduced the general SEW angle which allows us to analyze the behavior of the conventional SEW angle but with an arbitrary reference direction function. A special choice of the reference direction function, the stereographic SEW angle, reduces the effect of the coordinate singularity as compared to the conventional SEW angle. The stereographic SEW angle allows the use of more of the workspace without encountering singularities. Even at a singularity, the arm can have continuous joint movement as long as a smooth path is taken directly through the singularity. We have shown that since an algorithmic singularity is unavoidable for any choice of parameterization of the redundant degree of freedom, the stereographic SEW angle is ideal in that it only encounters a singularity when the wrist is at a half-line from the shoulder.

We have also used the subproblem decomposition method to provide IK solutions for most known 7R robots. These solutions are often closed-form and may sometimes require a 1D or 2D search. This method finds all IK solutions and finds least-squares solutions for some robots as well. We provide IK solutions for both common robots as well as robots that do not seem to be manufactured yet, such as an R-R-3R||-2R arm. Furthermore, we are the first to demonstrate solving IK by finding a high-order polynomial in the tangent half-angle for 7R arms parameterized by the general SEW angle.

In the future, it would be interesting to further investigate resolving redundancy given this new parameterization, that is, picking the ideal trajectory for the stereographic SEW angle. It may also be worthwhile to further investigate IK for more types of 7R robots using the subproblem decomposition approach.

There has been a recent surge of literature on cuspidal robots, which are robots that can travel between inverse kinematics solutions without encountering a singularity [84]. To the best of our knowledge, nobody has defined cuspidality for redundant manipulators or determined which redundant manipulators are cuspidal. There are many theorems for cuspidal non-redundant manipulators that need to be reevaluated to see if they apply to redundant manipulators as well.

CRediT authorship contribution statement

Alexander J. Elias: Conceptualization, Methodology, Software, Validation, Investigation, Writing - Original Draft, Writing - Review & Editing, Visualization. **John T. Wen:** Methodology, Writing - Review & Editing, Supervision, Project administration.

Declaration of competing interest

The authors declare that they have no known competing financial interests or personal relationships that could have appeared to influence the work reported in this paper.

Data availability

No data was used for the research described in the article.

Supplementary materials

Supplementary material associated with this article can be found at `https://www.youtube.com/@AlexEliasRobotics`.

Table of Multimedia Extensions

Extension	Media Type	Description
1	Video	Comparing conventional and stereographic SEW angles
2	Video	Sawyer inverse kinematics solutions using 1D search

References

[1] Robotics Research Corporation, Dexterous manipulators and advanced control systems (2005).
[2] Rethink Robotics, Baxter User Guide (2015).
[3] Rethink Robotics, Intera 5 - User Guide/Getting Started (2018).
[4] ABB, Product manual - IRB 14000 (2023).
[5] C. D. Crane III, J. Duffy, T. Carnahan, A kinematic analysis of the space station remote manipulator system (SSRMS), Journal of Robotic Systems 8 (5) (1991) 637–658.
[6] J. M. Hollerbach, Optimum kinematic design for a seven degree of freedom manipulator, in: Robotics research: The second international symposium, Citeseer, 1985, pp. 215–222.
[7] Y. Chen, X. Zhang, Y. Huang, Y. Wu, J. Ota, Kinematics optimization of a novel 7-DOF redundant manipulator, Robotics and Autonomous Systems 163 (2023) 104377.
[8] F. Flacco, A. De Luca, O. Khatib, Motion control of redundant robots under joint constraints: Saturation in the null space, in: 2012 IEEE International Conference on Robotics and Automation, IEEE, 2012, pp. 285–292.
[9] J. M. Hollerbach, K. Suh, Redundancy resolution of manipulators through torque optimization, IEEE Journal on Robotics and Automation 3 (4) (1987) 308–316.
[10] Y. Tsumaki, P. Fiorini, G. Chalfant, H. Seraji, A numerical SC approach for a teleoperated 7-DOF manipulator, in: Proceedings 2001 ICRA. IEEE International Conference on Robotics and Automation (Cat. No. 01CH37164), Vol. 1, IEEE, 2001, pp. 1039–1044.
[11] J. W. R. Pryor, Teleoperation methods for high-risk, high-latency environments, Ph.D. thesis, Johns Hopkins University (2023).
[12] X. Zhu, X. Wang, Y. Ma, Design and development of teleoperation interactive system for 7-DOF space redundant manipulator, in: 2021 5th International Conference on Automation, Control and Robots (ICACR), IEEE, 2021, pp. 179–183.
[13] P. L. Swaim, J. J. Arend, P. J. Bevill, R. J. Decker, J. C. Dunn, D. A. Read, R. E. Reiher, B. J. Richard, K. J. Ruta, S. Teplitz, Use of manipulators in assembly of space station freedom, in: S. B. Skaar (Ed.), Teleoperation and robotics in space, Vol. 161 of Progress in Astronautics and Aeronautics, American Institute of Aeronautics and Astronautics, Inc., Washington, DC, 1994, Ch. 16, pp. 443–473.
[14] Yaskawa, Motoman-SIA50D Instructions (2014).
[15] E. Dupuis, A general framework for the manual teleoperation of kinematically redundant space-based manipulators, Ph.D. thesis, McGill University (2001).
[16] C. R. Carignan, R. D. Howard, A partitioned redundancy management scheme for an eight-joint revolute manipulator, Journal of Robotic Systems 17 (9) (2000) 453–468.
[17] C. R. Carignan, J. C. Lane, P. J. Churchill, Controlling robots on-orbit, in: Proceedings 2001 IEEE International Symposium on Computational Intelligence in Robotics and Automation (Cat. No. 01EX515), IEEE, 2001, pp. 314–319.
[18] M. Naylor, E. Atkins, S. Roderick, Visual target recognition and tracking for autonomous manipulation tasks, in: AIAA Guidance, Navigation and Control Conference and Exhibit, 2007, p. 6323.
[19] N. A. Scott, C. R. Carignan, A line-based obstacle avoidance technique for dexterous manipulator operations, in: 2008 IEEE International Conference on Robotics and Automation, IEEE, 2008, pp. 3353–3358.
[20] A. J. Elias, J. T. Wen, IK-Geo: Unified robot inverse kinematics using subproblem decomposition, arXiv preprint arXiv:2211.05737v3 (2024).
[21] D. L. Pieper, The kinematics of manipulators under computer control, Stanford University, 1969.
[22] J. Baillieul, Kinematic programming alternatives for redundant manipulators, in: Proceedings. 1985 IEEE International Conference on Robotics and Automation, Vol. 2, IEEE, 1985, pp. 722–728.
[23] J. Burdick, H. Seraji, Characterization and control of self-motions in redundant manipulators, in: Proceedings of the NASA Conference on Space Telerobotics, Volume 2, 1989, pp. 3–14.
[24] K. Kreutz-Delgado, M. Long, H. Seraji, Kinematic analysis of 7 DOF anthropomorphic arms, in: Proceedings., IEEE International Conference on Robotics and Automation, IEEE, 1990, pp. 824–830.
[25] K. Kreutz-Delgado, M. Long, H. Seraji, Kinematic analysis of 7-DOF manipulators, The International Journal of Robotics Research 11 (5) (1992) 469–481.
[26] B. Stanczyk, A. Peer, M. Buss, Development of a high-performance haptic telemanipulation system with dissimilar kinematics, Advanced robotics 20 (11) (2006) 1303–1320.
[27] J. Baillieul, J. Hollerbach, R. Brockett, D. Martin, R. Percy, R. Thomas, Kinematically redundant robot manipulators, in: Proceedings of the Workshop on Space Telerobotics, Vol. 2, Jet Propulsion Lab., California Inst. of Tech., 1987, pp. 245–255.
[28] K. O'Neil, Y.-C. Chen, Instability of pseudoinverse acceleration control of redundant mechanisms, in: Proceedings 2000 ICRA. Millennium Conference. IEEE International Conference on Robotics and Automation. Symposia Proceedings (Cat. No. 00CH37065), Vol. 3, IEEE, 2000, pp. 2575–2582.
[29] H. Seraji, Configuration control of redundant manipulators: Theory and implementation, IEEE Transactions on Robotics and Automation 5 (4) (1989) 472–490.
[30] C. Lamperti, A. M. Zanchettin, P. Rocco, A redundancy resolution method for an anthropomorphic dual-arm manipulator based on a musculoskeletal criterion, in: 2015 IEEE/RSJ International Conference on Intelligent Robots and Systems (IROS), IEEE, 2015, pp. 1846–1851.
[31] H. Su, J. Sandoval, M. Makhdoomi, G. Ferrigno, E. De Momi, Safety-enhanced human-robot interaction control of redundant robot for teleoperated minimally invasive surgery, in: 2018 IEEE International Conference on Robotics and Automation (ICRA), IEEE, 2018, pp. 6611–6616.
[32] H. Su, J. Sandoval, P. Vieyres, G. Poisson, G. Ferrigno, E. De Momi, Safety-enhanced collaborative framework for tele-operated minimally invasive surgery using a 7-DoF torque-controlled robot, International Journal of Control, Automation and Systems 16 (2018) 2915–2923.
[33] H. Su, C. Yang, G. Ferrigno, E. De Momi, Improved human–robot collaborative control of redundant robot for teleoperated minimally invasive surgery, IEEE Robotics and Automation Letters 4 (2) (2019) 1447–1453.
[34] ABB, Technical reference manual - System parameters RW7 (2024).
[35] Yaskawa, Motoman-SIA5D/SIA5F Instructions (2017).

[36] KUKA, LBR iiwa 14 R820, datasheet (2022).
[37] G. Xiong, Y. Zhou, J. Yao, Null-space impedance control of 7-degree-of-freedom redundant manipulators based on the arm angles, International Journal of Advanced Robotic Systems 17 (3) (2020) 1729881420925297.
[38] B. Stanczyk, M. Buss, Development of a telerobotic system for exploration of hazardous environments, in: 2004 IEEE/RSJ International Conference on Intelligent Robots and Systems (IROS)(IEEE Cat. No. 04CH37566), Vol. 3, IEEE, 2004, pp. 2532–2537.
[39] K.-K. Lee, M. Buss, Redundancy resolution with multiple criteria, in: 2006 IEEE/RSJ International Conference on Intelligent Robots and Systems, IEEE, 2006, pp. 598–603.
[40] H. Kim, L. M. Miller, A. Al-Refai, M. Brand, J. Rosen, Redundancy resolution of a human arm for controlling a seven DOF wearable robotic system, in: 2011 Annual International Conference of the IEEE Engineering in Medicine and Biology Society, IEEE, 2011, pp. 3471–3474.
[41] H. Kim, L. M. Miller, N. Byl, G. M. Abrams, J. Rosen, Redundancy resolution of the human arm and an upper limb exoskeleton, IEEE Transactions on Biomedical Engineering 59 (6) (2012) 1770–1779.
[42] Z. Li, J. R. Roldan, D. Milutinović, J. Rosen, The rotational axis approach for resolving the kinematic redundancy of the human arm in reaching movements, in: 2013 35th Annual International Conference of the IEEE Engineering in Medicine and Biology Society (EMBC), IEEE, 2013, pp. 2507–2510.
[43] Y. Wang, P. Artemiadis, Closed-form inverse kinematic solution for anthropomorphic motion in redundant robot arms, Advances in Robotics and Automation 2 (3) (2013).
[44] W. Liu, D. Chen, J. Steil, Analytical inverse kinematics solver for anthropomorphic 7-DOF redundant manipulators with human-like configuration constraints, Journal of Intelligent & Robotic Systems 86 (1) (2017) 63–79.
[45] H. Su, N. Enayati, L. Vantadori, A. Spinoglio, G. Ferrigno, E. De Momi, Online human-like redundancy optimization for tele-operated anthropomorphic manipulators, International Journal of Advanced Robotic Systems 15 (6) (2018) 1729881418814695.
[46] C. Wang, L. Peng, Z.-G. Hou, J. Li, L. Luo, S. Chen, W. Wang, Kinematic redundancy analysis during goal-directed motion for trajectory planning of an upper-limb exoskeleton robot, in: 2019 41st Annual International Conference of the IEEE Engineering in Medicine and Biology Society (EMBC), IEEE, 2019, pp. 5251–5255.
[47] S. Li, K. Han, P. He, Z. Li, Y. Liu, Y. Xiong, Human-like redundancy resolution: An integrated inverse kinematics scheme for anthropomorphic manipulators with radial elbow offset, Advanced Engineering Informatics 54 (2022) 101812.
[48] L. Yan, Z. Mu, W. Xu, Analytical inverse kinematics of a class of redundant manipulator based on dual arm-angle parameterization, in: 2014 IEEE International Conference on Systems, Man, and Cybernetics (SMC), IEEE, 2014, pp. 3744–3749.
[49] H. H. An, W. I. Clement, B. Reed, Analytical inverse kinematic solution with self-motion constraint for the 7-DOF restore robot arm, in: 2014 IEEE/ASME International Conference on Advanced Intelligent Mechatronics, IEEE, 2014, pp. 1325–1330.
[50] M. Shimizu, W.-K. Yoon, K. Kitagaki, A practical redundancy resolution for 7 DOF redundant manipulators with joint limits, in: Proceedings 2007 IEEE International Conference on Robotics and Automation, IEEE, 2007, pp. 4510–4516.
[51] L. Jiang, X. Huo, Y. Liu, H. Liu, An integrated inverse kinematic approach for the 7-DOF humanoid arm with offset wrist, in: 2013 IEEE International Conference on Robotics and Biomimetics (ROBIO), IEEE, 2013, pp. 2737–2742.
[52] B. Tondu, A closed-form inverse kinematic modelling of a 7R anthropomorphic upper limb based on a joint parametrization, in: 2006 6th IEEE-RAS International Conference on Humanoid Robots, IEEE, 2006, pp. 390–397.
[53] T. Nammoto, K. Kosuge, An analytical solution for a redundant manipulator with seven degrees of freedom, International Journal of Automation and Smart Technology 2 (4) (2012) 339–346.
[54] A. Sinha, N. Chakraborty, Geometric search-based inverse kinematics of 7-DoF redundant manipulator with multiple joint offsets, in: 2019 International Conference on Robotics and Automation (ICRA), IEEE, 2019, pp. 5592–5598.
[55] M. Pfurner, Closed form inverse kinematics solution for a redundant anthropomorphic robot arm, Computer Aided Geometric Design 47 (2016) 163–171.
[56] W. Xu, Y. She, Y. Xu, Analytical and semi-analytical inverse kinematics of SSRMS-type manipulators with single joint locked failure, Acta Astronautica 105 (1) (2014) 201–217.
[57] I. Zaplana, L. Basanez, A novel closed-form solution for the inverse kinematics of redundant manipulators through workspace analysis, Mechanism and machine theory 121 (2018) 829–843.
[58] M. Gong, X. Li, L. Zhang, Analytical inverse kinematics and self-motion application for 7-DOF redundant manipulator, IEEE Access 7 (2019) 18662–18674.
[59] X. Tian, Q. Xu, Q. Zhan, An analytical inverse kinematics solution with joint limits avoidance of 7-DOF anthropomorphic manipulators without offset, Journal of the Franklin Institute 358 (2) (2021) 1252–1272.
[60] C. Faria, F. Ferreira, W. Erlhagen, S. Monteiro, E. Bicho, Position-based kinematics for 7-DoF serial manipulators with global configuration control, joint limit and singularity avoidance, Mechanism and Machine Theory 121 (2018) 317–334.
[61] Y. Wang, C. Zhao, X. Wang, P. Zhang, P. Li, H. Liu, Inverse kinematics of a 7-DOF spraying robot with 4R 3-DOF non-spherical wrist, Journal of Intelligent & Robotic Systems 101 (4) (2021) 1–17.
[62] B. Ma, Z. Xie, Z. Jiang, H. Liu, Precise semi-analytical inverse kinematic solution for 7-DOF offset manipulator with arm angle optimization, Frontiers of Mechanical Engineering 16 (3) (2021) 435–450.
[63] J. Zhao, X. Yang, Z. Zhao, G. Yang, L. Zhao, Inverse kinematics and multi-objective configuration optimization of the SSRMS manipulator, Advances in Space Research (2023).
[64] M. Jin, Q. Liu, B. Wang, H. Liu, An efficient and accurate inverse kinematics for 7-DOF redundant manipulators based on a hybrid of analytical and numerical method, IEEE Access 8 (2020) 16316–16330.
[65] FANUC, Datasheet R-1000iA/120F-7B (2019).
[66] X. Shi, Y. Guo, X. Chen, Z. Chen, Z. Yang, Kinematics and singularity analysis of a 7-DOF redundant manipulator, Sensors 21 (21) (2021) 7257.
[67] S. Chiaverini, Singularity-robust task-priority redundancy resolution for real-time kinematic control of robot manipulators, IEEE Transactions on Robotics and Automation 13 (3) (1997) 398–410.

[68] G. Marani, J. Kim, J. Yuh, W. K. Chung, Algorithmic singularities avoidance in task-priority based controller for redundant manipulators, in: Proceedings 2003 IEEE/RSJ International Conference on Intelligent Robots and Systems (IROS 2003)(Cat. No. 03CH37453), Vol. 4, IEEE, 2003, pp. 3570–3574.
[69] Z. Wang, K. Kazerounian, Identification and resolution of structural and algorithmic singularity in redundancy control of serial manipulations, Journal of robotic systems 12 (7) (1995) 465–478.
[70] Y. Choi, Y. Oh, S. R. Oh, J. Park, W. K. Chung, Multiple tasks manipulation for a robotic manipulator, Advanced Robotics 18 (6) (2004) 637–653.
[71] D. H. Gottlieb, Robots and fibre bundles, Bull. Soc. Math. Belg 38 (1986) 219–223.
[72] P. McGrath, An extremely short proof of the hairy ball theorem, The American Mathematical Monthly 123 (5) (2016) 502–503.
[73] H. Poincaré, Sur les courbes définies par les équations différentielles, J. Math. Pures Appl. 4 (1885) 167–244.
[74] H. Hopf, Vektorfelder inn-dimensionalen mannigfaltigkeiten, Mathematische Annalen 96 (1) (1927) 225–249.
[75] T. Needham, Visual complex analysis, Oxford University Press, 1997.
[76] T. Debus, S. Dougherty, Overview and performance of the front-end robotics enabling near-term demonstration (FREND) robotic arm, in: AIAA Infotech@Aerospace Conference and AIAA Unmanned...Unlimited Conference, 2009, p. 1870.
[77] R. Mukherji, D. A. Ray, M. Stieber, J. Lymer, Special purpose dexterous manipulator (SPDM) advanced control features and development test results, Proceedings of the 6th International Symposium on Artificial Intelligence, Robotics and Automation in Space (i-SAIRAS) (2001).
[78] R. Boumans, C. Heemskerk, The European robotic arm for the international space station, Robotics and Autonomous systems 23 (1-2) (1998) 17–27.
[79] D. Arney, J. Mulvaney, C. Williams, C. Stockdale, N. Gelin, P. le Gouellec, In-space servicing, assembly, and manufacturing (ISAM) state of play, Tech. rep., Consortium for Space Mobility and ISAM Capabilities (COSMIC) (2023).
[80] Productive Robots, OB7 Collaborative Robot User Manual (2018).
[81] Franka Emika, Franka Production 3 Product Manual (2022).
[82] Ufactory, UFACTORY xArm User Manual (2023).
[83] Universal Robots, User Manual UR5/CB3 (2021).
[84] P. Wenger, D. Chablat, A review of cuspidal serial and parallel manipulators, Journal of Mechanisms and Robotics 15 (4) (2023) 040801.